Cell wall integrity and elicitor peptide signaling modulate jasmonic acid-mediated camalexin production in Arabidopsis

Richard Noi Morton[1], Lian Fleischberger[1], Joy Debnath[2], David Biermann[3], Susanne Mühlbauer[4], Ahalya Rajendran[1,#], Hans-Henning Kunz[4], Julien Gronnier[3], Nora Gigli Bisceglia[2] and Timo Engelsdorf[1]*

[1]Molecular Plant Physiology, Department of Biology, Philipps-Universität Marburg, 35043 Marburg, Germany

[2]Plant Stress Resilience, Institute of Environmental Biology, Utrecht University, 3584 Utrecht, Netherlands

[3]Plant Cell Biology, TUM School of Life Sciences, Technical University of Munich, 85354 Freising, Germany

[4]Plant Biochemistry and Physiology, LMU Munich, 82152 Martinsried-Planegg, Germany

[#]present address: Department of Biochemistry, Max Planck Institute for Chemical Ecology, 07745 Jena, Germany.

*Corresponding author: Email: timo.engelsdorf@uni-marburg.de

Summary

Plant cell walls constitute dynamic barriers that are essential for defense against pathogens. The receptor kinase THESEUS1 (THE1) monitors cell wall integrity (CWI) and contributes to pathogen resistance in Arabidopsis, but the underlying mechanisms remain unclear. Here we show that THE1-dependent CWI signaling induces accumulation of the antimicrobial metabolite camalexin upon cell wall damage (CWD) caused by cellulose biosynthesis inhibition or fungal infection. CWD alters THE1 plasma membrane nanodomain organization and involves calcium signaling components that modulate camalexin production. Induction of camalexin requires jasmonic acid (JA)-dependent expression of the transcription factors MYB47 and MYB95. In line with its antagonistic function on CWI signaling, the plant elicitor peptide Pep3 suppresses camalexin biosynthesis downstream of THE1 by inhibiting JA-dependent pathways. Our findings reveal a regulatory network where CWI and Pep3 signaling modulate antimicrobial defense via JA-mediated camalexin production. This network requires independent CWD-induced pathways, providing insights into how plants balance defense activation and suppression in response to cell wall stress.

Key words

Cell wall integrity, pathogen resistance, receptor kinase THESEUS1, jasmonic acid signaling, camalexin biosynthesis, plant elicitor peptides, calcium signaling, isoxaben, *Arabidopsis thaliana*

Introduction

Cell walls provide mechanical support to plant cells and serve as sturdy, yet highly dynamic barriers against plant pathogen infection. The ability of pathogens to modify host cell wall properties and to locally breach the barrier determines their successful entry into host tissues and their virulence on specific host plants (Bhandari et al., 2025; Munzert and Engelsdorf, 2025). Consequently, specific alterations in cell wall composition and structure influence the outcome of plant-pathogen interactions (Molina et al., 2021; Reckleben et al., 2025). It is well established that immune signaling is increased in many cell wall mutants and accumulating evidence suggests that signaling pathways induced by cell wall damage (CWD) contribute to pathogen defense (Bacete et al., 2018; Vaahtera et al., 2019). The cell wall status is constantly surveilled by a number of overlapping processes together referred to as cell wall signaling (Wolf, 2022). Cell wall stress correlates with the expression of small signaling peptides, which can influence cell wall properties (Debnath et al., 2026). Receptor kinases of the *Catharanthus roseus* receptor-like kinase 1-like (*Cr*RLK1L) family have a prominent role in cell wall signaling during development, growth, damage and immunity (Franck et al., 2018; Ortiz-Morea et al., 2022; Wolf, 2022). *Cr*RLK1Ls are receptors for RAPID ALKALINIZATION FACTOR (RALF) family peptides, which are central regulators of *Cr*RLK1L signaling (Schoenaers and Vissenberg, 2025). The *Cr*RLK1L THESEUS1 (THE1) is required for the induction of responses to CWD, e.g. in cellulose-deficient mutants, after cellulose biosynthesis inhibition with isoxaben (ISX) or after enzymatic cell wall degradation (Hématy et al., 2007; Engelsdorf et al., 2018; Bacete et al., 2022). Binding of RALF34 to THE1 contributes to regulation of lateral root initiation but is dispensable for THE1-dependent responses to ISX (Gonneau et al., 2018). Signaling responses induced by CWD are referred to as cell wall integrity (CWI) signaling (Vaahtera et al., 2019; Wolf, 2022). Responses to ISX include the reactive oxygen species (ROS)- and calcium-dependent induction of phytohormone production and ectopic cell wall lignification (Hamann et al., 2009; Denness et al., 2011). These responses depend on THE1 and the receptor kinases MALE DISCOVERER 1-INTERACTING RECEPTOR LIKE KINASE 2 (MIK2) and STRUBBELIG (Van der Does et al., 2017; Chaudhary et al., 2020). THE1 and MIK2 have partially overlapping functions in CWI signaling and both contribute to defense against the soilborne fungus *Fusarium oxysporum* (Van der Does et al., 2017). MIK2 is the receptor for SERINE-RICH ENDOGENOUS PEPTIDEs (SCOOPs) that regulate immunity and senescence (Hou et al., 2021; Rhodes et al., 2021; Zhang et al., 2024). ISX-induced CWD promotes SCOOP expression in a partially THE1-dependent manner, which increases responses to a subsequent treatment with pathogen-associated molecular patterns (PAMPs) (Zhai et al., 2024). This highlights how signals originating from a damaged cell wall can contribute to pattern-triggered immunity (PTI). Intriguingly, loss of PTI elements such as BRASSINOSTEROID INSENSITIVE 1 (BRI1)–ASSOCIATED KINASE 1 (BAK1), BAK1-LIKE

1 (BKK1), BOTRYTIS-INDUCED KINASE 1 (BIK1), PEP1 RECEPTOR 1 (PEPR1) and PEPR2 leads to increased ISX responses, indicating that PTI can negatively regulate CWI signaling (Engelsdorf et al., 2018).

PTI's feedback inhibition of CWI signaling depends on endogenous plant elicitor peptides (Peps) that are perceived by PEPR1/2 and BAK1 (Yamaguchi et al., 2006; Yamaguchi et al., 2010; Tang et al., 2015). Pep1 and Pep3 precursor genes, *PROPEP1* and *PROPEP3*, are induced in a THE1-independent manner after 1 hour of ISX treatment and co-treatment of seedlings with ISX and synthetic Pep1 or Pep3 suppresses ISX-induced accumulation of the phytohormones jasmonic acid (JA) and salicylic acid (SA) (Engelsdorf et al., 2018). *PROPEPs* are also induced by wounding, salinity, pathogen infection or PAMP treatments, but the direct stimulus leading to their expression is unknown (Bartels and Boller, 2015; Nakaminami et al., 2018). Salinity-induced *PROPEP3* expression is alleviated by treatments that affect cell wall crosslinking, indicating that stress-induced changes in cell wall properties may play a role (Gigli-Bisceglia et al., 2022). Overexpression of *PROPEP1* and *PROPEP3* is sufficient to rescue plants from cell death after long-term treatment with ISX or growth under high salinity, demonstrating their impact on stress resistance (Nakaminami et al., 2018; Zhang et al., 2025). Cellular damage activates calcium-, SUMOylation- and metacaspase-dependent PROPEP processing and released Peps can spread danger signals to neighboring cells (Hander et al., 2019; Shen et al., 2019; Zhang et al., 2025).

In summary, the state of the art suggests that THE1-dependent CWI monitoring can contribute to basal defense against pathogen infection (Guerreiro and Marhavý, 2023). Basal defense against pathogens involves the production of phytohormones and of specialized antimicrobial metabolites, termed phytoalexins (Bari and Jones, 2009; Ahuja et al., 2012). In Arabidopsis, the major phytoalexin camalexin is synthesized by a metabolon comprising several Cytochrome P450 enzymes, whose expression is regulated by WRKY transcription factors (Birkenbihl et al., 2012; Birkenbihl et al., 2017; Mucha et al., 2019). During fungal infections, camalexin is produced and secreted locally at infection sites to restrict fungal proliferation (Glawischnig, 2007; He et al., 2019).

Here, we investigated the mechanism by which camalexin biosynthesis is activated and regulated upon CWD through THE1-dependent CWI signaling and how this defense response is negatively regulated by Pep3 signaling. Our findings elucidate the interplay between these pathways in modulating antimicrobial defense in Arabidopsis.

Results

THE1 contributes to camalexin accumulation and pathogen resistance

To investigate how THE1-mediated CWI signaling contributes to pathogen resistance, we infected the *the1-1* loss of function mutant with the hemibiotrophic fungus *Colletotrichum higginsianum*, which depends on host cell wall penetration, causing local CWD (O'Connell et al., 2004; Engelsdorf et al., 2017). The fungal entry rate was significantly increased in *the1-1*, indicating that CWI signaling contributes to defense at this early infection step (Figure 1A). To identify antimicrobial defense responses linked to CWD, we examined publicly available transcriptomics data and found that genes encoding for Cytochrome P450 enzymes involved in camalexin biosynthesis are strongly upregulated after ISX-induced CWD (Hamann et al., 2009; Figure S1). Previous research demonstrated that camalexin-deficiency caused by loss of *CYP71B15/PAD3* or *WRKY33*, a major positive regulator of camalexin biosynthesis, critically weakens resistance against *C. higginsianum* (Narusaka et al., 2004; Mao et al., 2011; Schmidt et al., 2020). Indeed, camalexin accumulation was reduced in *the1-1* after *C. higginsianum* infection, indicating that THE1 contributes to induction of camalexin biosynthesis upon CWD caused by fungal infection (Figure 1B). To further investigate the importance of impaired camalexin accumulation for *the1-1* susceptibility, we crossed *the1-1* with the camalexin-deficient *pad3* mutant and quantified fungal genomic DNA during the necrotrophic growth phase, when colonization of surrounding tissue is increased in *pad3* (Narusaka et al., 2004). Fungal DNA was significantly increased in *the1-1*, *pad3* and *the1-1 pad3* compared to Col-0 wild type, but not significantly different between single and double mutants, indicating overlapping effects of THE1 and camalexin synthesis on pathogen resistance (Figure 1C).

Cell wall damage is sufficient to induce THE1-dependent camalexin accumulation

The finding that THE1 played a role in camalexin induction during pathogen entry through the cell wall prompted us to investigate if CWI impairment is sufficient to induce camalexin biosynthesis. ISX treatments are ideally suited to further investigate the regulation of CWD-induced camalexin biosynthesis, as treatments can be performed in seedling liquid culture in a controlled and well-established manner separating CWD from other molecular events that occur during plant-pathogen interactions (Paredez et al., 2006; Gutierrez et al., 2009). Consistent with transcriptional activation of camalexin biosynthesis, ISX treatments of 10 days old seedlings induced camalexin accumulation after 8 hours (Figure 2A). We have previously shown that treatment of Arabidopsis seedlings with Driselase, a mixture of cell wall-degrading enzymes, induces similar CWI responses as ISX treatment (Engelsdorf et al., 2018). In line with that, camalexin accumulation was increased after Driselase treatment compared to heat-inactivated Driselase, indicating that camalexin accumulation is induced by different types of

151 CWD (Figure S2). Stress-induced conversion of the key indolic intermediate indole-3-
152 acetaldoxime (IAOx) to indole-3- acetonitrile (IAN) for camalexin biosynthesis depends on the
153 two cytochrome P450 enzymes CYP71A12 and CYP71A13, with stronger contribution of the
154 latter (Müller et al., 2015). Transcriptional data indicated that *CYP71A12* was already induced
155 after 4 hours ISX treatment, whereas *CYP71A13* was upregulated 8 hours after ISX treatment,
156 following a similar expression pattern as *CYP71B15/PAD3*, the final enzyme in camalexin
157 biosynthesis (Figure S1). Loss of CYP71A13 completely abolished ISX-induced camalexin
158 accumulation, while loss of CYP71A12 increased camalexin accumulation (Figure 2B). This
159 data shows that CYP71A13 is essential for ISX-induced camalexin biosynthesis, whereas
160 CYP71A12 rather diverges IAOx into other pathways such as indole-3-carboxylic acid (ICA)
161 synthesis (Pastorczyk et al., 2020). To investigate if CWD-induced camalexin biosynthesis
162 depends on THE1, we quantified camalexin in ISX-treated *the1-1* seedlings and found that
163 camalexin accumulation was completely abolished in the mutant (Figure 2C). Consistently,
164 treatment of the hypermorphic *the1-4* allele (Merz et al., 2017) caused increased camalexin
165 accumulation (Figure 2C). Camalexin accumulation was abolished in an ISX-treated *wrky33*
166 mutant and close to the detection limit in *the1-4 wrky33* double mutants, showing that the major
167 transcriptional regulator of camalexin biosynthesis, WRKY33, is necessary for ISX-induced,
168 THE1-dependent camalexin synthesis (Figure 2D).
169
170 **Calcium signaling determines the magnitude of ISX-induced camalexin response**
171 Previous studies demonstrated that Ca^{2+} signaling is required for ISX-induced JA accumulation
172 (Denness et al., 2011) and that Ca^{2+} transients are involved in CWI maintenance under high
173 salinity (Feng et al., 2018). Consistently, blocking of calcium channels with $LaCl_3$ during ISX
174 treatments indicated that Ca^{2+} signaling is required for ISX-induced camalexin accumulation
175 (Figure 2E). To resolve which channels and Ca^{2+} sensing mechanisms contribute to this
176 response, we investigated mutants for the plasma membrane localized channel MATING
177 PHEROMONE INDUCED DEATH 1 (MID1)–COMPLEMENTING ACTIVITY 1 (MCA1), which
178 has been previously implicated in mechanosensing and CWI signaling (Nakagawa et al., 2007;
179 Engelsdorf et al., 2018), and the chloroplast localized CALCIUM SENSING RECEPTOR
180 (CAS), which is required for the regulation of cytosolic Ca^{2+} transients upon external Ca^{2+}
181 signals (Nomura et al., 2008; Weinl et al., 2008). Camalexin accumulation in response to ISX
182 treatment was reduced by 60 and 47 % in *cas* and *mca1* mutants, respectively, supporting that
183 both genes contribute to CWD responses (Figure 2F). Stress-induced Ca^{2+} transients occur in
184 the cytosol and in the chloroplast stroma (Nomura et al., 2012). To test whether altered
185 distribution between stromal and cytosolic Ca^{2+} influences ISX responses, we investigated
186 camalexin production in double mutants of the PLASTID ENVELOPE ION CHANNELs (PEC1,
187 PEC2) that exhibit reduced stromal and increased cytosolic Ca^{2+} transients after stress

188 exposure (Völkner et al., 2021). ISX treatment induced higher camalexin accumulation in *pec1*
189 *pec2* than in Col-0, indicating that increased cytosolic Ca^{2+} transients promote the CWD
190 response (Figure 2G). The importance of Ca^{2+} at a later stage (hours) of CWD might indicate
191 that Ca^{2+} signaling is influenced by CWI status. To test this idea, we used high salinity and ice-
192 cold water, two independent stimuli inducing cell wall stress (Debnath et al., 2026), to elicit
193 cytosolic Ca^{2+} transients in Col-0 and *pec1 pec2* seedlings that had been pretreated with mock
194 or ISX. Both treatments caused increased cytosolic Ca^{2+} peaks in ISX- compared to mock-
195 treated seedlings, indicating that CWD increases the sensitivity for Ca^{2+} elicitation (Figure 2H,I;
196 Figure S3).
197
198 **Pep3-triggered signaling inhibits CWI signaling downstream of THE1**
199 We have previously reported that ISX-induced, THE1-dependent phytohormone responses are
200 negatively regulated by Pep1 and Pep3, however the underlying mechanism remained
201 unknown (Engelsdorf et al., 2018). To investigate how Pep perception affects ISX-induced
202 camalexin accumulation, we treated Col-0, *pepr1 pepr2* and *bak1-5 bkk1* seedlings with ISX,
203 Pep3 and a combination of both. We chose Pep3 for this study, (i) because it attenuates THE1-
204 dependent phytohormone accumulation, but, unlike Pep1, does not induce ectopic root
205 lignification, and (ii) because we previously demonstrated that PROPEP3 is secreted upon cell
206 wall damage (Engelsdorf et al., 2018). Pep3 co-treatment led to suppression of ISX-induced
207 camalexin accumulation in a PEPR- and BAK1/BKK1-dependent manner (Figure 3A),
208 indicating that Pep3 inhibits THE1-dependent camalexin synthesis via PEPR-mediated
209 signaling.
210 Despite the recognized function of THE1 as a CWI sensor, little is known about its regulation
211 upon perception of CWD. Accumulating reports link changes in the plasma membrane protein
212 organization with the initiation of cell signaling (Jaillais et al., 2024). We combined enhanced
213 super-resolution radial fluctuation (eSRRF) (Laine et al., 2023) with variable-angle total internal
214 reflection microscopy (VA-TIRFM) imaging (Konopka and Bednarek, 2008) to analyze the
215 plasma membrane organization of THE1-GFP upon CWD. We observed that a subpopulation
216 of THE1-GFP was organized into nanodomains and that 1 hour and 6 hours of ISX treatment
217 led to a decrease in the density of THE1-GFP nanodomains (Figure 3B,C). Congruently, the
218 relative proportion of THE1-GFP localization organized in nanodomains and the image-wide
219 spatial clustering index (iSCI) of THE1-GFP were reduced at both time points after ISX
220 treatment (Figure S4). Confocal microscopy showed that THE1-GFP localization to the plasma
221 membrane was unaffected by ISX treatment (Figure S5). Together, these data indicate that
222 THE1-GFP is spatially redistributed within the plasma membrane upon CWD induced by ISX
223 and may indicate that THE1-GFP nanodomains correspond to resting pools of the receptor
224 that are released for function. To test whether the Pep3-dependent suppression of THE1-

225 mediated camalexin synthesis could be linked to altered THE1 localization, we treated THE1-
226 GFP seedlings with ISX, Pep3 and a combination of both. Neither the mean THE1-GFP
227 fluorescence at the plasma membrane nor THE1 nanodomain organization were altered by
228 Pep3 co-treatment, suggesting that negative regulation of ISX responses is exerted
229 downstream of THE1 (Figure 3B,C, Figure S4, Figure S5). In good agreement with this
230 conclusion, suppression of ISX-induced camalexin by Pep3 was also observed in the
231 hypermorphic *the1-4* allele (Figure 3D).
232
233 **Pep3-dependent inhibition of CWI responses is independent from WRKY33 and MPK3/6**
234 To investigate if Pep3 inhibition of CWI signaling downstream of THE1 involves transcriptional
235 regulation of *WRKY33* or *PAD3*, we performed time course qRT-PCR analysis in Col-0, *the1-*
236 *1*, *the1-4* and *pepr1 pepr2* mutants. Pep3 treatment led to upregulation of *WRKY33* after 2
237 hours, whereas *PAD3* expression was not induced at this time point (Figure S6). ISX caused
238 the upregulation of *WRKY33* between 2 and 4 hours after treatment and of *PAD3* between 4
239 and 6 hours after treatment (Figure S6). Notably, ISX-induced *WRKY33* induction was neither
240 significantly affected by THE1, nor by Pep3 co-treatment (Figure 4A). Instead, *PAD3* induction
241 after ISX treatment was reduced in *the1-1,* increased in *the1-4* and suppressed by Pep3 co-
242 treatment, showing that THE1 and Pep3 regulate *PAD3* without influencing *WRKY33*
243 expression (Figure 4B).
244 We previously reported that the MAP kinase kinase kinase (MAPKKK) family proteins
245 Arabidopsis NPK1-related Protein kinase 1 (ANP1) and ANP3 regulate ISX-dependent
246 responses, indicating that MAP kinase signaling plays a role in CWI signaling (Gigli Bisceglia
247 et al., 2018). Camalexin accumulation after pathogen infection involves phosphorylation of
248 WRKY33 by the MAP kinases MPK3 and MPK6, both of which are phosphorylated by Pep3-
249 triggered signaling (Mao et al., 2011; Bartels et al., 2013). To test if MPK3/6 are involved in
250 ISX-induced camalexin synthesis and/or in Pep3-dependent inhibition of the same, we
251 analyzed camalexin levels in Col-0, *mpk3* and *mpk6* seedlings after treatment with mock,
252 Pep3, ISX and ISX+Pep3. MPK3, but not MPK6, was required for ISX-induced camalexin
253 accumulation (Figure 4C). We were however unable to detect any changes in MPK3/6
254 phosphorylation after ISX treatment for 10 min, when CESAs are internalized (Paredez et al.,
255 2006), as well as after 4 and 6 hours, when transcriptional responses become more
256 pronounced and phytohormones and camalexin start to accumulate (Denness et al., 2011;
257 Engelsdorf et al., 2018; Zhai et al., 2024) (Figure S7). While Pep3 single or combined
258 treatments induced MPK3 and MPK6 phosphorylation (Figure S7), Pep3-dependent
259 suppression of ISX-induced camalexin accumulation was not affected in *mpk3* and *mpk6*
260 mutants, suggesting that MPK3/6 signaling is not required for Pep3-triggered inhibition of CWI
261 responses (Figure 4C).

262 Taken together, our data indicate that Pep3-PEPR signaling inhibits ISX-induced production of
263 camalexin downstream of THE1 and independent from MPK3/6 and WRKY33.
264
265 **MYB and WRKY transcription factors are regulated by THE1 and Pep3 signaling**
266 To identify candidate genes that mediate Pep3 inhibition of CWI signaling, we performed RNA-
267 Sequencing of Col-0 seedlings treated with mock, Pep3, ISX and ISX+Pep3 for 6 hours, when
268 *PAD3* expression was suppressed by the co-treatment (Figure 4B). Principal component
269 analysis showed that biological replicates grouped according to treatments and indicated that
270 the largest share of the transcriptional changes in the data sets could be explained by ISX
271 treatment (Figure S8A). Hierarchical cluster analysis supported this conclusion by grouping
272 ISX and ISX+Pep3 treatments together but also revealed groups of genes with opposite
273 expression patterns between both treatments (Figure S8B). Analysis of differential gene
274 expression identified a total of 543 genes significantly downregulated (α=0.05, fold change >
275 2) after Pep3 (89 genes), ISX (330) and ISX+Pep3 (313) treatment compared to mock control
276 (Figure 5A). Instead, 1513 genes were upregulated (α=0.05, fold change > 2) after treatment
277 with Pep3 (416 genes), ISX (1248) and ISX+Pep3 (1104) (Figure 5B). The transcription factors
278 *MYB47*, *MYB95*, *MYB113* and *WRKY67* were significantly upregulated by ISX, but not after
279 combined ISX+Pep3 treatment, making them candidates for mediating the negative effect of
280 Pep3 on CWI signaling. Quantitative RT-PCR showed that all four candidates were induced in
281 a THE1-dependent manner, with significantly increased expression in ISX-treated *the1-4* and
282 reduced expression in *the1-1* compared to the wild type (Figure 5C-F). *MYB47*, *MYB95* and
283 *MYB113* expression were mildly reduced by loss of *WRKY33*, whereas *WRKY67* expression
284 was increased in *wrky33*, *the1-1 wrky33* and *the1-4 wrky33* compared to Col-0 and *the1* single
285 mutants, respectively (Figure 5C-F). To investigate if MYB47 and the closely related MYB95
286 (Millard et al., 2019) are involved in the regulation of ISX-dependent camalexin accumulation
287 by Pep3, we subjected *myb47* single and *myb47/95* double mutants to mock, Pep3, ISX and
288 combined ISX and Pep3 treatments. We detected significantly reduced camalexin levels after
289 ISX treatment in both lines, indicating that MYB47 is required for induction of camalexin
290 biosynthesis, with no obvious contribution of MYB95 (Figure 5G,H). Congruently, the ISX-
291 induced expression of *PAD3* was significantly reduced in *myb47* and *myb47/95* seedlings,
292 whereas the induction of *CYP71A13* was only reduced in *myb47/95* seedlings (Figure 5I,J).
293 Two independent mutant lines for *MYB113* did not cause significant changes in camalexin
294 accumulation compared to WT (Figure S9). We also obtained three independent T-DNA
295 insertion lines for *WRKY67*, of which only SALK_073815 (now termed *wrky67-1*) displayed
296 reduced gene expression after ISX treatment, but no change in ISX-induced camalexin
297 accumulation (Figure S9).

298 Taken together, our RNA-Seq analysis identified four transcription factors that were induced in
299 a THE1-dependent manner and suppressed by Pep3 co-treatment, of which *MYB47* and
300 *MYB95* were required for the regulation of camalexin biosynthesis after CWD induction by ISX
301 treatment.
302
303 **MYB47/95 mediate THE1-induced and Pep3-sensitive JA signaling**
304 Previous research connected JA to camalexin biosynthesis induction and demonstrated that
305 JA accumulation in response to ISX treatment is sensitive to Pep signaling (Denness et al.,
306 2011; Engelsdorf et al., 2018; Zhou et al., 2022). This overlap prompted us to investigate the
307 role of JA in ISX-induced camalexin production and its Pep3-dependent negative regulation.
308 Our transcriptomics data showed an increased expression of genes involved in JA
309 biosynthesis, signaling and catabolism after 6 hours of ISX treatment, reduced expression after
310 6 hours Pep3 treatment, and an attenuated expression profile after combined ISX+Pep3
311 treatment compared to ISX treatment alone (Figure 6A). JA-deficient *aos* mutants did not
312 accumulate camalexin after ISX treatment, supporting an essential role of JA (Figure 6B).
313 Since JA induction after ISX treatment is attenuated by Pep3 (Engelsdorf et al., 2018), we
314 hypothesized that exogenous application of JA might abrogate Pep3-dependent suppression
315 of camalexin production. Indeed, triple treatment with ISX, Pep3 and JA strongly induced
316 camalexin accumulation, demonstrating that JA application is sufficient to override the negative
317 influence of Pep3 (Figure 6C).
318 Next, we investigated if ISX-induced expression of *MYB47*, *MYB95*, *MYB113* and *WRKY67*
319 depends on JA biosynthesis. Quantitative RT-PCR showed that ISX-dependent induction of
320 *MYB47*, *MYB113* and *WRKY67* was abolished and induction of *MYB95* attenuated in JA-
321 deficient *aos* mutants (Figure 6D-G). ISX-induced expression of *WRKY33* was independent of
322 JA and MYB47/95 (Figure 6H,I). Together, our data support a model in which THE1-dependent
323 CWI surveillance induces camalexin via JA and MYB47/95, whereas an independent pathway
324 induces *WRKY33* upon CWD (Figure 6J).
325
326 **Discussion**
327 In this study, we investigated contributions of THE1-dependent CWI signaling to the induction
328 of the phytoalexin camalexin and its interaction with Pep3 signaling. We show that CWI
329 impairment caused by cellulose biosynthesis inhibition, enzymatic cell wall degradation or
330 fungal infection induces camalexin accumulation. In line with the previously described role of
331 WRKY33 as central regulator of camalexin biosynthesis (Mao et al., 2011), increased CWI
332 signaling in the hypermorphic *the1-4* mutant required WRKY33 for camalexin induction.
333 WRKY33 expression was induced by ISX treatment, but was neither dependent on THE1, nor
334 affected by co-treatment with Pep3. This is in contrast with ISX-induced expression of PAD3,

335 catalyzing the final step of camalexin synthesis, which strongly depended on THE1 and was
336 suppressed by co-treatment with Pep3. Phosphorylation by MPK3/6 and CALCIUM-
337 DEPENDENT PROTEIN KINASEs (CPK5/6) controls WRKY33 DNA binding, autoactivation,
338 and transactivation of key camalexin biosynthesis genes (Zhou et al., 2020). Our analysis
339 showed that MPK3 controls ISX-induced camalexin accumulation, while MPK6 was not
340 required. MPK3 phosphorylation was not detectable at 10 minutes, 4 hours and 6 hours after
341 ISX treatment, indicating that (i) MPK phosphorylation after ISX treatment is not a fast
342 response, and (ii) that it may represent a transient and/or dynamic response that is difficult to
343 catch.
344 The importance of calcium signaling for ISX-induced CWD responses has long been
345 recognized (Denness et al., 2011), but the exact mode of action remains elusive. Current
346 evidence suggests that MCA1 might represent a stretch-activated Ca^{2+} channel required for
347 THE1-dependent CWI signaling (Nakagawa et al., 2007; Engelsdorf et al., 2018). Delayed
348 inhibitor treatment assays with $LaCl_3$ showed that calcium signaling affects responses to ISX
349 treatment that occur in the scale of hours, when CWD causes mechanical damage and
350 microscopically visible phenotypes (Denness et al., 2011; Engelsdorf et al., 2018; Bacete et
351 al., 2022). Congruently, $LaCl_3$ treatment abolished ISX-induced camalexin accumulation. Loss
352 of MCA1 halved camalexin levels compared to wild type, indicating that it may be partially
353 responsible for Ca^{2+} influx after CWD. Similarly, CAS, a chloroplast-localized positive regulator
354 of Ca^{2+} responses in the cytosol and the chloroplast stroma (Nomura et al., 2008; Weinl et al.,
355 2008; Nomura et al., 2012), contributed to camalexin accumulation in response to ISX. Loss
356 of chloroplast inner envelope ion channels PEC1/2 impairs stromal Ca^{2+} transients but
357 increases cytosolic Ca^{2+} transients, suggesting that Ca^{2+} is partially excluded from plastids
358 (Völkner et al., 2021). Our data indicate that increased cytosolic Ca^{2+} in *pec1/2* triggered ISX-
359 induced camalexin accumulation. While CWI maintenance during high salinity requires the
360 *Cr*RLK1L FER to induce late Ca^{2+} transients (Feng et al., 2018), *fer* mutants exhibit
361 constitutively increased CWD responses that cannot be alleviated by loss of THE1 (Engelsdorf
362 et al., 2018; Gonneau et al., 2018), indicating that different Ca^{2+} signatures might be involved
363 in CWI maintenance and CWD responses. We provide first hints that CWD increases
364 responsiveness to cell wall-related Ca^{2+} elicitation as ISX treated seedlings responded
365 stronger to high salinity and cold treatments. It will be interesting to investigate in the future if
366 CWI sensors contribute to this response.
367 In recent years, plasma membrane localized proteins have been recognized to be dynamically
368 organized in specific nanodomains according to developmental programs and stress
369 responses (Bücherl et al., 2017; Hdedeh et al., 2025). Protoplast cell wall regeneration assays
370 indicated that the cell wall influences lateral mobility of plasma membrane proteins and
371 chemical treatments affecting cellulose biosynthesis or pectin methylation caused changes in

372 protein nanodomain size and dynamics (Martinière et al., 2012; McKenna et al., 2019). These
373 changes might influence signaling, as the nanodomain organization of RLKs is influenced by
374 FER, cell wall localized LRR-EXTENSIN (LRX) and their ligand RALF23 (Gronnier et al., 2022;
375 Liu et al., 2024). In line with its central function in CWI signaling upon CWD, THE1 was spatially
376 reorganized at the plasma membrane after one hour of ISX treatment, showing that THE1
377 reorganization precedes accumulation of phytohormones and camalexin. This observation
378 suggests that THE1 may be released from nanodomains for function. Similarly, during viral
379 infection, the solicitation of REMORIN proteins correlates with their spatial redistribution and
380 an overall increase in their lateral diffusion (Perraki et al., 2018; Jolivet et al., 2025). Because
381 ligand-induced signaling can influence nanodomain organization of other receptor kinases
382 (Gronnier et al., 2022), we considered the possibility that Pep3 signaling may influence THE1
383 nanodomain organization. However, we observed no effects of Pep3 treatments on THE1-GFP
384 nanodomains under mock or ISX conditions, indicating interaction of CWI and Pep3 pathways
385 downstream of THE1. Consistently, we observed that Pep3 inhibited ISX-induced camalexin
386 accumulation in the hypermorphic *the1-4* allele.
387 To identify potential downstream regulators, we performed transcriptomics and discovered four
388 candidate transcription factors that were induced by ISX treatment in a THE1-dependent
389 manner and suppressed by Pep3 co-treatment, indicating that they are downstream of a Pep3-
390 THE1 pathway interaction. Mutant analysis revealed that *MYB47* and *MYB95* are required for
391 the induction of camalexin biosynthesis upon ISX treatment, extending the network of
392 transcription factors known to be involved in the regulation of the camalexin pathway. MYB34,
393 MYB51 and MYB122 regulate *CYP79B2* and *CYP79B3*, thereby affecting the conversion of
394 tryptophan to IAOx and determining precursor availability for camalexin synthesis (Frerigmann
395 et al., 2015). Instead, ANAC042, ERF1B and ERF72 are required for transcriptional induction
396 of *CYP71A13* and *PAD3*, directly regulating the camalexin biosynthesis pathway (Saga et al.,
397 2012; Li et al., 2021; Zhou et al., 2022; Monsalvo et al., 2025). Of note, ERF1B cooperates
398 with WRKY33 to induce camalexin pathway genes and is induced by JA (Zhou et al., 2022).
399 These properties are reminiscent of THE1 signaling in response to CWD, which induces the
400 JA pathway and acts in parallel to WRKY33 in camalexin synthesis. Indeed, JA was required
401 for ISX-induced camalexin accumulation as well as for induction of *MYB47*, *MYB95*, *MYB113*
402 and *WRKY67.* In Arabidopsis roots, cellulose defects cause cortex cell bulging and
403 compression of inner tissues stimulating JA signaling (Mielke et al., 2021). The same
404 mechanism might be responsible for JA induction after ISX treatment, where THE1 is required
405 for CWD detection. *MYB47* induction was previously detected in drought treated Arabidopsis
406 plants, where it was associated with increased JA signaling and drought stress survival
407 (Marquis et al., 2022). Since drought stress impairs CWI (Novaković et al., 2018), it would be
408 interesting to test if *MYB47* expression upon drought is induced by THE1-dependent CWI

signaling. Recently, Cao et al. (2025) reported that *MYB47* is induced by JA and increases JA catabolism in leaves, thereby delaying leaf senescence. Bizan et al. (2025) showed that *MYB47* and *MYB95* are controlled by master transcription factors of JA signaling, MYC2/3/4, and regulate a specific subset of JA-responsive genes related to ER-body formation and defense against fungal and insect infection. JA treatment alone was not sufficient to induce camalexin synthesis, and the available data indicates that at least two independent pathways need to be activated upon CWD to initiate this defense response (Zhou et al., 2022). Consistently, negative regulation of JA synthesis by Pep3 treatment was sufficient to suppress the camalexin pathway whereas JA application overrode the suppressive effect of Pep3 on ISX-induced camalexin accumulation.

Taken together, perception of CWD involves changes in THE1 nanodomain organization at the plasma membrane and regulation of Ca^{2+} signaling via MCA1, CAS and PEC (Figure 6J). THE1-induced JA signaling and THE1-independent WRKY33 are both induced by CWD and required for camalexin accumulation. Negative regulation of this cell wall-mediated defense response by PEPR-mediated perception of Pep3 is placed upstream of JA. We identified *MYB47*, *MYB95*, *MYB113* and *WRKY67* as ISX-induced, THE1- and JA-dependent transcription factors, of which *MYB47* and *MYB95* were required for the regulation of ISX-induced camalexin biosynthesis. We propose that the induction of camalexin production by CWD may contribute to defense at fungal penetration sites. In turn, current evidence suggests that Peps are released upon plasma membrane rupture allowing their binding to PEPRs of neighboring cells (Hander et al., 2019; Shen et al., 2019). Pep3 detection may therefore signify damage on the tissue level, leading to suppression of local cell wall-mediated defense at infection sites.

Materials and Methods

Plant materials and growth conditions

Arabidopsis thaliana genotypes used in this study are listed in Supplemental Table S1. Accession Columbia-0 (Col-0) was used as wild type in all experiments. All Arabidopsis mutants used in this study were either obtained from the Nottingham Arabidopsis Stock Centre (http://arabidopsis.info/), from laboratories where data on them has been published, or have been crossed from those.

For growth in sterile liquid culture, seeds were surface sterilized for 10 minutes with 70 % (v/v). The ethanol was subsequently replaced with a sterilizing solution of 2% sodium hypochlorite with 0.1 % Triton X-100, treated for additional 3 minutes and finally rinsed four times with sterile water. Seeds were then stratified at 4°C for 3 days before transfer to half-strength Murashige and Skoog liquid medium [Murashige and Skoog Basal Medium (2.1 g/liter), MES salt (0.5 g/liter), and 1 % sucrose, pH 5.7]. Unless stated otherwise, seedling cultures were established

446 in a 24-well plate with 6 seeds per well. Seedlings were grown under a 16-hour light (22°C) /
447 8-hour dark (20°C) cycle and a photon flux density of 110 µmol m^{-2} s^{-1}.
448 For growth on soil, Arabidopsis seeds were placed on a mixture of 80 % Fruhstorfer Type P
449 (Hawita, Germany) and 20 % Liadrain clay (Liapor, Germany), stratified for 3 days and grown
450 at a photon flux density of 110 µmol m^{-2} s^{-1} under the light cycles indicated in the figure
451 legends.
452
453 Plant liquid culture treatments
454 Unless stated otherwise, 10-day-old seedlings were subjected to the following treatments in
455 fresh liquid growth medium at the indicated final concentrations: 600 nM isoxaben (ISX;
456 Supelco 36138), 10 nM *At*Pep3, 600 nM ISX + 10 nM *At*Pep3 (combined treatment of ISX and
457 AtPep3), 10 mM $LaCl_3$, 5 µM jasmonic acid (JA; Cayman Chemical 88300), 600 nM ISX + 10
458 nM *At*Pep3 + 5 µM JA (combined treatment of ISX, *At*Pep3, and JA). Equal amounts of DMSO
459 were present in all treatments, including mock treatments. Treatment with 0.03 % (w/v)
460 Driselase (Dri; Sigma-Aldrich D8037) and inactivated (bDri) was performed according to
461 Engelsdorf et al. (2018). After treatment, seedlings were briefly rinsed, patted dry, snap-frozen
462 in liquid nitrogen and stored at -70°C until further analysis. *At*Pep3
463 (EIKARGKNKTKPTPSSGKGGKHN) was custom synthesized and supplied by EZBiolab Inc.
464 (Indiana, USA).
465
466 *Colletotrichum higginsianum* infection assays
467 *Colletotrichum higginsianum* isolate MAFF 305635 (Ministry of Forestry and Fisheries, Japan)
468 was used for all infection experiments. Conidia were plated on oatmeal agar (5 % [w/v]
469 shredded oatmeal, 1.2 % [w/v] agar) and incubated for 7 days in a 16 h light (22°C) / 8 h dark
470 (20°C) cycle at a photon flux density of 110 µmol m^{-2} s^{-1}. Immediately prior to infection, conidia
471 were harvested by rinsing plates with deionized water and the titer was adjusted to $2 \cdot 10^6$
472 conidia ml^{-1}. Spray infection of leaf rosettes was performed at the end of the light phase and
473 high humidity maintained until 2.5 days post infection to support fungal penetration as
474 described (Voll et al., 2012). Fungal entry rates were determined by microscopic examination
475 after staining fungal structures with trypan blue as described in Engelsdorf et al. (2017) and
476 quantification of the relative fungal DNA content in infected leaves was performed by qPCR
477 analysis of *ChTrpC* as described in Engelsdorf et al. (2013).
478
479 Quantitative reverse transcription polymerase chain reaction (qRT-PCR)
480 Total RNA was isolated using a NucleoSpin Plant and Fungi RNA Mini Kit (Macherey-Nagel).
481 One microgram of total RNA was treated with RNase-Free DNase (Thermo Scientific) and
482 used for complementary DNA (cDNA) synthesis with a RevertUP II Reverse Transcriptase Kit

483 (Biotechrabbit). Quantitative reverse transcription polymerase chain reaction (qRT-PCR) was
484 performed using Blue S'Green (Biozym) SYBR green mix and a Bio-Rad CFX Connect RT-
485 PCR system. Primers are listed in Supplemental Table S2. *ACT2* was used a reference in all
486 experiments.
487
488 RNA-Sequencing
489 Total RNA was isolated using a NucleoSpin Plant and Fungi RNA Mini Kit (Macherey-Nagel)
490 and shipped to Novogene Europe (Cambridge, UK) for further processing. RNA integrity was
491 assessed using the RNA Nano 6000 Assay Kit of the Bioanalyzer 2100 system (Agilent
492 Technologies, CA, USA). Total RNA was used as input material for the RNA sample
493 preparations. Briefly, mRNA was purified from total RNA using poly-T oligo-attached magnetic
494 beads. Fragmentation was carried out using divalent cations under elevated temperature in
495 First Strand Synthesis Reaction Buffer (5X). First strand cDNA was synthesized using random
496 hexamer primer and M-MuLV Reverse Transcriptase (RNase H-). Second strand cDNA
497 synthesis was subsequently performed using DNA Polymerase I and RNase H. Remaining
498 overhangs were converted into blunt ends via exonuclease/polymerase activities. After
499 adenylation of 3' ends of DNA fragments, adaptors with hairpin loop structure were ligated to
500 prepare for hybridization. To select cDNA fragments of preferentially 370~420 bp in length, the
501 library fragments were purified with AMPure XP system (Beckman Coulter, Beverly, USA).
502 PCR was performed with Phusion High-Fidelity DNA polymerase using universal and index
503 PCR primers, PCR products were purified (AMPure XP system), and library quality was
504 assessed on the Agilent Bioanalyzer 2100 system. The clustering of the index-coded samples
505 was performed on a cBot Cluster Generation System using TruSeq PE Cluster Kit v3-cBot-HS
506 (Illumina) according to the manufacturer's instructions. After cluster generation, the library
507 preparations were sequenced on an Illumina Novaseq platform and 150 bp paired-end reads
508 were generated. Raw data (raw reads) of fastq format were firstly processed through in-house
509 perl scripts. In this step, clean data (clean reads) were obtained by removing reads containing
510 adapter, reads containing poly-N and low-quality reads from raw data. All the downstream
511 analyses were based on the clean data with high quality. Index of the TAIR10 reference
512 genome was built using Hisat2 v2.0.5 and paired-end clean reads were aligned to the
513 reference genome using Hisat2 v2.0.5. Differential expression analysis was performed using
514 the DESeq2 R package (1.20.0). The resulting p-values were adjusted using the Benjamini
515 and Hochberg's approach for controlling the false discovery rate. Genes with an adjusted p-
516 value <=0.05 found by DESeq2 and a fold change > 2 were assigned as differentially
517 expressed.
518
519

520 Camalexin quantification

521 To analyze camalexin content in seedlings grown in liquid culture, whole seedlings were
522 freeze-dried for 17 hours using the CHRIST ALPHA 2-4 system (Martin Christ, Osterode am
523 Harz, Germany) and their dry weight recorded. For *Colletotrichum higginsianum*-infected leaf
524 material, camalexin was directly extracted from sampled leaf discs as described (Nawrath and
525 Métraux, 1999; Engelsdorf et al., 2013). Crude phytochemicals were extracted from the
526 samples in 600 µl 70 % methanol supplemented with 50 ng ortho-anisic acid (oANI) as internal
527 standard at 65°C for 1 hour. Crude extraction was repeated on the same samples with 90 %
528 methanol at 65°C for 1 hour. The two extractions were combined, and a rotatory vacuum
529 concentrator (RVC 2-25 CDplus, Martin Christ) was used to evaporate methanol. Proteins and
530 other biomolecules were precipitated from the extract with 500 µl of 5 % trichloroacetic acid.
531 After centrifugation, the supernatant was collected into a fresh reaction tube and partitioned
532 twice against 600 µl of cyclohexane/ethyl acetate (1:1 (v/v)) solution with vigorous shaking and
533 centrifugation at 3,500*g* for 10 min. The combined organic (upper) phases were evaporated in
534 the vacuum concentrator and resuspended in 80 % 25 mM potassium dihydrogen phosphate
535 buffer (25 mM KH_2PO_4, pH 2.6) / 20% acetonitrile (ACN). Camalexin content in the extract was
536 separated on an InfinityLab Poroshell 120 EC-C18 (3.0 x 150 mm 2.7-Micron, Agilent
537 Technologies) column and analyzed using an UHPLC system (1260 Infinity II, Agilent
538 Technologies, Santa Clara, California, USA). The separation was achieved using gradient
539 elution of a mobile phase consisting of (A) 25 mM KH_2PO_4, pH 2.6, and (B) 99 % ACN in water
540 at a flow rate of 1 ml/min: 0 – 2.5 min: 20 % B; 2.5 – 6 min: 20 % to 80 % B; 6 – 7 min: 80 %
541 B; 7 – 8 min: 80 % to 20 % B; 8–10 min: 20 % B. The G712B fluorescence detector (Agilent
542 Technologies) was used to detect oANI (excitation 305 nm, emission 365 nm) and camalexin
543 (excitation 305 nm, emission 370 nm). A standard dilution series of oANI and camalexin in the
544 range of 0.02 to 100 ng was employed for quantification. OpenLAb CDS ChemStation software
545 C01.10 (Agilent Technologies) was used to operate the HPLC system and to analyze the data.
546

547 MAP kinase phosphorylation assay

548 Seedlings were grown in half-strength Murashige and Skoog (MS) liquid medium [Murashige
549 and Skoog Basal Medium (2.1 g/L), MES (0.5 g/L), and 1 % sucrose, pH 5.7] in 12-well plates.
550 On the ninth day, the medium was replaced with fresh medium, and on the following day
551 seedlings were treated with either Mock (DMSO), 600 nM ISX, 10 nM *At*Pep3, or a combined
552 treatment of 600 nM ISX + 10 nM *At*Pep3 for 10 min, 4 hours, or 6 hours. Protein extraction
553 was performed as described in Gigli-Bisceglia et al. (2022). For protein extraction, the following
554 buffer was used: 50 mM Tris-HCl (pH 7.5), 200 mM NaCl, 1 mM EDTA, 10 % (v/v) glycerol, 0.1
555 % (v/v) Tween 20, 1 mM PMSF, 1 mM DTT, 1× protease inhibitor cocktail (Sigma-Aldrich,
556 P9599), and 1× phosphatase inhibitor cocktail (Sigma-Aldrich, P2850). Samples were

incubated on ice for 15 min and centrifuged at 13,000 g for 15 min at 4°C. The resulting supernatants were used for western blot analysis. Protein concentration was determined using the Bradford assay (Bio-Rad). Samples were mixed with 4× loading buffer [240 mM Tris-HCl (pH 6.8), 8 % (w/v) SDS, 40 % glycerol, 5 % β-mercaptoethanol, 0.04 % (w/v) Bromophenol Blue] and heated at 95°C for 2 min. Protein samples (35 µg total protein per lane) were separated on 10 % SDS-PAGE gels and transferred to nitrocellulose membranes using the Trans-Blot Turbo Transfer System (Bio-Rad) at 25 V, 1.3 A for 7 min. Membranes were blocked in Tris-buffered saline with 0.1 % Tween 20 (TBST) containing 5 % (w/v) bovine serum albumin (BSA; Sigma-Aldrich, A3608) for 1 h, then incubated overnight with the primary phospho-p44/42 MAPK (Erk1/2) (Thr202/Tyr204) antibody (1:2000, Cell Signaling Technology, 9101). After three washes with TBST, membranes were incubated with the secondary HRP-linked anti-rabbit IgG antibody (1:6000, Cell Signaling Technology, 7074) for 2 hours. Following three additional washes with TBST, chemiluminescence was detected using Clarity Western ECL Substrate (Bio-Rad, 1705061) for 2 min and visualized with the ChemiDoc imaging system (Bio-Rad). For equal loading analysis, membranes were stripped using stripping solution (100 mM Tris-HCl, pH 6.8, 2 % SDS, 100 mM β-mercaptoethanol) for 1 hour at 60°C, re-blocked as described above, and probed with the β-Actin (C4) antibody (1:2000, Santa Cruz Biotechnology, sc-47778) for 1 hour. Following three washes (TBST), chemiluminescence detection was performed as described previously.

<u>Ca^{2+} assays</u>

To monitor cytosolic Ca^{2+} transients, we employed Arabidopsis reporter lines expressing cytosolic-targeted aequorin in Col-0 (pMAQ2; Knight et al., 1991) and *pec1-1 pec2-1* background (unpublished). The measurements were carried out as described before by Tanaka et al. (2013), with minor alterations. Briefly, seedlings (5 days old) grown sterilely on half-strength Murashige and Skoog (½ MS) medium were transferred into white 96-well plates, each well containing 50 µL of coelenterazine buffer (10 µM coelenterazine, 1.4 mM $CaCl_2$, 20 mM KCl, 5 mM MES-KOH, pH 5.7). For aequorin reconstitution, seedlings were kept in the dark at 22 °C overnight. For priming experiments, ISX was added at a final concentration of 600 nM 4.5 hours prior to the measurement. Cytosolic Ca^{2+} transients were elicited with 200 mM NaCl or ice-cold water. Luminescence was recorded using a TECAN Spark plate reader (Tecan, Männedorf, Switzerland), with an integration time of 500 ms. To determine total aequorin content, seedlings were discharged using 10% ethanol (v/v) and 1 M $CaCl_2$. Calcium levels were calculated from luminescence signals as described by (Knight et al., 1996).

Confocal microscopy

Five-day old Arabidopsis seedlings grown on solid ½ MS, 1% Sucrose, 0.8 % Agar, pH 5.8 plates under a 16-hour photoperiod were incubated in ½ MS pH 5.8 liquid solutions containing 600 nM isoxaben, 10 nM *At*Pep3, a combination of both or corresponding mock controls for the indicated durations. Seedlings were mounted in the same solution they were treated in and imaged using a Leica SP8 confocal microscope equipped with a HC PL 10x/0.3 objective, a white light laser and HyD detectors. GFP was excited using 488 nm wavelength and fluorescence emission was detected between 495 nm and 535 nm. Acquisition parameters were kept constant during experiments. Fluorescence intensity was measured using Fiji (Schindelin et al., 2012).

Variable angle-total internal reflection microscopy (VA-TIRFM)

Arabidopsis seedlings were grown and treated as described for confocal microscopy. Five-day old seedlings were mounted in the same solution they were treated in between two coverslips and imaged using a custom-build microscope platform for variable angle total internal reflection microscopy (VA-TIRFM) (Rohr et al., 2024), equipped with an 100x objective NA 1.49 (Zeiss, 421190-9800-000), a polychromatic modulator (AOTF, AA OPTO-ELECTRONIC) and a sCMOS camera (Hamamatsu Photonics, ORCA-Flash4.0 V2). To ensure that the target laser power value always corresponds to the actual irradiance in the sample plane, the power of each laser line was calibrated before each experiment using a PM100D detector (Thorlabs) as previously described (von Arx et al., 2024). Samples were excited with 488 nm diode laser at 200 µW and 20 seconds stream acquisitions were recorded at 5 Hz for each cell. Acquisition parameters were kept constant during experiments.

Enhanced-super resolution radial fluctuation analyses (eSRRF)

Super-resolved image reconstructions of THE1-GFP plasma membrane organization were computed using eSRRF (Laine et al., 2023) in Fiji (Schindelin et al., 2012). Stream VA-TIRFM acquisitions were processed using the following parameters that were defined by iterative parameter sweep (Laine et al., 2023): magnification = 6, radius = 3, sensitivity = 3 and frames = 100. The average (AVG) reconstructions of THE1-GFP plasma membrane organization were segmented and analysed using Nanonet, an automated custom-made analysis pipeline (https://github.com/NanoSignalingLab/NanoNet), providing nanodomain density and image wide spatial clustering index (iSCI) based on predicted localization density.

Statistical analysis

All statistical analysis were performed with GraphPad Prism (Version 10.5.0). Specific information on statistical methods, sample size, significance level and p-values are provided in the respective figure legends.

Acknowledgements

This work was funded by the Deutsche Forschungsgemeinschaft (DFG, German Research Foundation) grants EN 1071/3-1 (to TE), A09-SFB1101 (to JG) and B01-TRR356 (to JG). H-HK and SM were supported by DFG SFB-TR 175, project B09 (INST 86/2119-2). NGB was supported by the Dutch Research Council (NWO) under grant numbers OCENW.M.24.079 and OCENW.XS23.1.050.

We are grateful to Debora Gasperini (IPB Halle) for providing *aos* seeds; Stefan Weinl and Jörg Kudla (Universität Münster) for *cas-1* seeds; Erich Glawischnig (TU Munich) for *cyp71a12/a13* seeds; and Kay Schneitz (TU Munich) for *pTHE1::THE1-GFP* seeds. Live cell imaging was performed at the ZMBP microscopy facility of the University of Tübingen and at the Center for Advanced Light Microscopy (CALM) of the TUM School of Life Sciences. We thank Michelle von Arx (TU Munich) for providing access to the NanoNet software prior publication and acknowledge Christiane Rohrbach and Nadja Braun (both Philipps-Universität Marburg) for excellent technical assistance.

Author contributions

Conceptualization and project administration: TE; Investigation: RNM, LF, JD, DB, SM, AR, NGB, TE; Funding acquisition: H-HK, JG, NGB, TE; Supervision: RNM, H-HK, JG, NGB, TE; Writing – original draft: TE; Writing – review & editing: RNM, LF, JD, DB, SM, AR, H-HK, JG, NGB, TE.

Declaration of interests

The authors declare no competing interests.

Data availability

The RNA-Seq data generated during this study have been deposited in the GEO repository (www.ncbi.nlm.nih.gov/geo/) under accession number GSE317084.

References

Ahuja I, Kissen R, Bones AM (2012) Phytoalexins in defense against pathogens. Trends in Plant Science **17:** 73-90

Bacete L, Mélida H, Miedes E, Molina A (2018) Plant cell wall-mediated immunity: Cell wall changes trigger disease resistance responses. The Plant Journal **93:** 614-636

Bacete L, Schulz J, Engelsdorf T, Bartosova Z, Vaahtera L, Yan G, Gerhold JM, Tichá T, Øvstebø C, Gigli-Bisceglia N, Johannessen-Starheim S, Margueritat J, Kollist H, Dehoux T,

McAdam SAM, Hamann T (2022) THESEUS1 modulates cell wall stiffness and abscisic acid production in *Arabidopsis thaliana*. Proceedings of the National Academy of Sciences **119:** e2119258119

Bari R, Jones JDG (2009) Role of plant hormones in plant defence responses. Plant Molecular Biology **69:** 473-488

Bartels S, Boller T (2015) Quo vadis, Pep? Plant elicitor peptides at the crossroads of immunity, stress, and development. Journal of Experimental Botany **66:** 5183-5193

Bartels S, Lori M, Mbengue M, van Verk M, Klauser D, Hander T, Böni R, Robatzek S, Boller T (2013) The family of Peps and their precursors in Arabidopsis: differential expression and localization but similar induction of pattern-triggered immune responses. Journal of Experimental Botany **64:** 5309-5321

Bhandari DD, Kim S-J, Brandizzi F (2025) Fortifying the frontier: cell wall modifications during plant immunity. Current Opinion in Plant Biology **88:** 102816

Birkenbihl RP, Diezel C, Somssich IE (2012) Arabidopsis WRKY33 Is a Key Transcriptional Regulator of Hormonal and Metabolic Responses toward Botrytis cinerea Infection Plant Physiology **159:** 266-285

Birkenbihl RP, Kracher B, Roccaro M, Somssich IE (2017) Induced Genome-Wide Binding of Three Arabidopsis WRKY Transcription Factors during Early MAMP-Triggered Immunity. The Plant Cell **29:** 20-38

Bizan J, Sarkar S, Basak AK, Bera S, Goto-Yamada S, Endo K, Tarnawska-Glatt K, Batth R, Bhardwaj K, Mirzaei M, Czerniawski P, Bednarek P, Yamada K (2025) Arabidopsis MYB47 and MYB95 transcription factors regulate jasmonate-inducible ER-body formation. Communications Biology **8:** 1377

Bücherl CA, Jarsch IK, Schudoma C, Segonzac C, Mbengue M, Robatzek S, MacLean D, Ott T, Zipfel C (2017) Plant immune and growth receptors share common signalling components but localise to distinct plasma membrane nanodomains. eLife **6:** e25114

Cao J, Yang Q, Zhao Y, Tan S, Li S, Cheng D, Zhang R, Zhang M, Li Z (2025) MYB47 delays leaf senescence by modulating jasmonate pathway via direct regulation of CYP94B3/CYP94C1 expression in Arabidopsis. New Phytologist **246:** 2192-2206

Chaudhary A, Chen X, Gao J, Leśniewska B, Hammerl R, Dawid C, Schneitz K (2020) The Arabidopsis receptor kinase STRUBBELIG regulates the response to cellulose deficiency. PLOS Genetics **16:** e1008433

Debnath J, Morton RN, Engelsdorf T, Gigli-Bisceglia N (2026) Plant Cell Wall Remodeling and Peptide Signaling Under Abiotic and Biotic Stress. Plant Communications

Denness L, McKenna JF, Segonzac C, Wormit A, Madhou P, Bennett M, Mansfield J, Zipfel C, Hamann T (2011) Cell wall damage-induced lignin biosynthesis is regulated by a reactive oxygen species- and jasmonic acid-dependent process in Arabidopsis. Plant Physiology **156:** 1364-1374

Engelsdorf T, Gigli-Bisceglia N, Veerabagu M, McKenna JF, Vaahtera L, Augstein F, Van der Does D, Zipfel C, Hamann T (2018) The plant cell wall integrity maintenance and immune signaling systems cooperate to control stress responses in *Arabidopsis thaliana*. Science Signaling **11**

Engelsdorf T, Horst RJ, Pröls R, Pröschel M, Dietz F, Hückelhoven R, Voll LM (2013) Reduced carbohydrate availability enhances the susceptibility of Arabidopsis toward *Colletotrichum higginsianum*. Plant Physiology **162:** 225-238

Engelsdorf T, Will C, Hofmann J, Schmitt C, Merritt BB, Rieger L, Frenger MS, Marschall A, Franke RB, Pattathil S, Voll LM (2017) Cell wall composition and penetration resistance against the fungal pathogen *Colletotrichum higginsianum* are affected by impaired starch turnover in Arabidopsis mutants. Journal of Experimental Botany **68:** 701-713

Feng W, Kita D, Peaucelle A, Cartwright HN, Doan V, Duan Q, Liu M-C, Maman J, Steinhorst L, Schmitz-Thom I, Yvon R, Kudla J, Wu H-M, Cheung AY, Dinneny JR (2018) The FERONIA receptor kinase maintains cell-wall integrity during salt stress through Ca^{2+} signaling. Current Biology **28:** 666-675.e665

Franck CM, Westermann J, Boisson-Dernier A (2018) Plant malectin-like receptor kinases: From cell wall integrity to immunity and beyond. Annual Review of Plant Biology **69:** 301-328

Frerigmann H, Glawischnig E, Gigolashvili T (2015) The role of MYB34, MYB51 and MYB122 in the regulation of camalexin biosynthesis in Arabidopsis thaliana. Frontiers in Plant Science **6:** 654

Gigli Bisceglia N, Savatin DV, Cervone F, Engelsdorf T, De Lorenzo G (2018) Loss of the Arabidopsis Protein Kinases ANPs Affects Root Cell Wall Composition, and Triggers the Cell Wall Damage Syndrome. Frontiers in Plant Science **8**

Gigli-Bisceglia N, van Zelm E, Huo W, Lamers J, Testerink C (2022) Arabidopsis root responses to salinity depend on pectin modification and cell wall sensing. Development **149:** dev200363

Glawischnig E (2007) Camalexin. Phytochemistry **68:** 401-406

Gonneau M, Desprez T, Martin M, Doblas VG, Bacete L, Miart F, Sormani R, Hématy K, Renou J, Landrein B, Murphy E, Van De Cotte B, Vernhettes S, De Smet I, Höfte H (2018) Receptor kinase THESEUS1 is a rapid alkalinization factor 34 receptor in Arabidopsis. Current Biology **28:** 2452-2458.e2454

Gronnier J, Franck CM, Stegmann M, DeFalco TA, Abarca A, von Arx M, Dünser K, Lin W, Yang Z, Kleine-Vehn J, Ringli C, Zipfel C (2022) Regulation of immune receptor kinase plasma membrane nanoscale organization by a plant peptide hormone and its receptors. eLife **11:** e74162

Guerreiro J, Marhavý P (2023) Unveiling the intricate mechanisms of plant defense. Frontiers in Plant Physiology **1:1285373**

Gutierrez R, Lindeboom JJ, Paredez AR, Emons AMC, Ehrhardt DW (2009) Arabidopsis cortical microtubules position cellulose synthase delivery to the plasma membrane and interact with cellulose synthase trafficking compartments. Nature Cell Biology **11:** 797

Hamann T, Bennett M, Mansfield J, Somerville C (2009) Identification of cell-wall stress as a hexose-dependent and osmosensitive regulator of plant responses. The Plant Journal **57:** 1015-1026

Hander T, Fernández-Fernández ÁD, Kumpf RP, Willems P, Schatowitz H, Rombaut D, Staes A, Nolf J, Pottie R, Yao P, Gonçalves A, Pavie B, Boller T, Gevaert K, Van Breusegem F, Bartels S, Stael S (2019) Damage on plants activates Ca2+-dependent metacaspases for release of immunomodulatory peptides. Science **363:** eaar7486

Hdedeh O, Mercier C, Poitout A, Martinière A, Zelazny E (2025) Membrane nanodomains to shape plant cellular functions and signaling. New Phytologist **245:** 1369-1385

He Y, Xu J, Wang X, He X, Wang Y, Zhou J, Zhang S, Meng X (2019) The Arabidopsis Pleiotropic Drug Resistance Transporters PEN3 and PDR12 Mediate Camalexin Secretion for Resistance to Botrytis cinerea. The Plant Cell **31:** 2206-2222

Hématy K, Sado P-E, Van Tuinen A, Rochange S, Desnos T, Balzergue S, Pelletier S, Renou J-P, Höfte H (2007) A receptor-like kinase mediates the response of Arabidopsis cells to the inhibition of cellulose synthesis. Current Biology **17:** 922-931

Hou S, Liu D, Huang S, Luo D, Liu Z, Xiang Q, Wang P, Mu R, Han Z, Chen S, Chai J, Shan L, He P (2021) The Arabidopsis MIK2 receptor elicits immunity by sensing a conserved signature from phytocytokines and microbes. Nature Communications **12:** 5494

Jaillais Y, Bayer E, Bergmann DC, Botella MA, Boutté Y, Bozkurt TO, Caillaud M-C, Germain V, Grossmann G, Heilmann I, Hemsley PA, Kirchhelle C, Martinière A, Miao Y, Mongrand S, Müller S, Noack LC, Oda Y, Ott T, Pan X, Pleskot R, Potocky M, Robert S, Rodriguez CS, Simon-Plas F, Russinova E, Van Damme D, Van Norman JM, Weijers D, Yalovsky S, Yang Z, Zelazny E, Gronnier J (2024) Guidelines for naming and studying plasma membrane domains in plants. Nature Plants **10:** 1172-1183

Jolivet M-D, Deroubaix AF, Boudsocq M, Abel NB, Rocher M, Robbe T, Wattelet-Boyer V, Huard J, Lefebvre D, Lu Y-J, Day B, Saias G, Ahmed J, Cotelle V, Giovinazzo N, Gallois J-L, Yamaji Y, German-Retana S, Gronnier J, Ott T, Mongrand S, Germain V (2025) Interdependence of plasma membrane nanoscale dynamics of a kinase and its cognate substrate underlies Arabidopsis response to viral infection. eLife **12:** RP90309

Knight H, Trewavas AJ, Knight MR (1996) Cold calcium signaling in Arabidopsis involves two cellular pools and a change in calcium signature after acclimation. The Plant Cell **8:** 489-503

Knight MR, Campbell AK, Smith SM, Trewavas AJ (1991) Transgenic plant aequorin reports the effects of touch and cold-shock and elicitors on cytoplasmic calcium. Nature **352:** 524-526

Konopka CA, Bednarek SY (2008) Variable-angle epifluorescence microscopy: a new way to look at protein dynamics in the plant cell cortex. The Plant Journal **53:** 186-196

Laine RF, Heil HS, Coelho S, Nixon-Abell J, Jimenez A, Wiesner T, Martínez D, Galgani T, Régnier L, Stubb A, Follain G, Webster S, Goyette J, Dauphin A, Salles A, Culley S, Jacquemet G, Hajj B, Leterrier C, Henriques R (2023) High-fidelity 3D live-cell nanoscopy through data-driven enhanced super-resolution radial fluctuation. Nature Methods **20:** 1949-1956

Li Y, Liu K, Tong G, Xi C, Liu J, Zhao H, Wang Y, Ren D, Han S (2021) MPK3/MPK6-mediated phosphorylation of ERF72 positively regulates resistance to Botrytis cinerea through directly and indirectly activating the transcription of camalexin biosynthesis enzymes. Journal of Experimental Botany **73:** 413-428

Liu M-CJ, Yeh F-LJ, Yvon R, Simpson K, Jordan S, Chambers J, Wu H-M, Cheung AY (2024) Extracellular pectin-RALF phase separation mediates FERONIA global signaling function. Cell **187:** 312-330.e322

Mao G, Meng X, Liu Y, Zheng Z, Chen Z, Zhang S (2011) Phosphorylation of a WRKY Transcription Factor by Two Pathogen-Responsive MAPKs Drives Phytoalexin Biosynthesis in Arabidopsis. The Plant Cell **23:** 1639-1653

Marquis V, Smirnova E, Graindorge S, Delcros P, Villette C, Zumsteg J, Heintz D, Heitz T (2022) Broad-spectrum stress tolerance conferred by suppressing jasmonate signaling attenuation in Arabidopsis JASMONIC ACID OXIDASE mutants. The Plant Journal **109:** 856-872

Martinière A, Lavagi I, Nageswaran G, Rolfe DJ, Maneta-Peyret L, Luu D-T, Botchway SW, Webb SED, Mongrand S, Maurel C, Martin-Fernandez ML, Kleine-Vehn J, Friml J, Moreau P, Runions J (2012) Cell wall constrains lateral diffusion of plant plasma-membrane proteins. Proceedings of the National Academy of Sciences **109:** 12805-12810

McKenna JF, Rolfe DJ, Webb SED, Tolmie AF, Botchway SW, Martin-Fernandez ML, Hawes C, Runions J (2019) The cell wall regulates dynamics and size of plasma-membrane nanodomains in Arabidopsis. Proceedings of the National Academy of Sciences **116:** 12857-12862

Merz D, Richter J, Gonneau M, Sanchez-Rodriguez C, Eder T, Sormani R, Martin M, Hématy K, Höfte H, Hauser M-T (2017) T-DNA alleles of the receptor kinase THESEUS1 with opposing effects on cell wall integrity signaling. Journal of Experimental Botany **68:** 4583-4593

Mielke S, Zimmer M, Meena MK, Dreos R, Stellmach H, Hause B, Voiniciuc C, Gasperini D (2021) Jasmonate biosynthesis arising from altered cell walls is prompted by turgor-driven mechanical compression. Science Advances **7:** eabf0356

Millard PS, Weber K, Kragelund BB, Burow M (2019) Specificity of MYB interactions relies on motifs in ordered and disordered contexts. Nucleic Acids Research **47:** 9592-9608

Molina A, Miedes E, Bacete L, Rodríguez T, Mélida H, Denancé N, Sánchez-Vallet A, Rivière M-P, López G, Freydier A, Barlet X, Pattathil S, Hahn M, Goffner D (2021) Arabidopsis cell wall composition determines disease resistance specificity and fitness. Proceedings of the National Academy of Sciences **118:** e2010243118

Monsalvo I, Parasecolo L, Pullano S, Lin J, Shahabi A, Ly M, Kwon H, Mathur K, Rodrillo KAM, Ifa DR, Kovinich N (2025) ANAC042 Regulates the Biosynthesis of Conserved- and Lineage-Specific Phytoalexins in Arabidopsis. International Journal of Molecular Sciences **26:** 3683

Mucha S, Heinzlmeir S, Kriechbaumer V, Strickland B, Kirchhelle C, Choudhary M, Kowalski N, Eichmann R, Hückelhoven R, Grill E, Kuster B, Glawischnig E (2019) The Formation of a Camalexin Biosynthetic Metabolon. The Plant Cell **31:** 2697-2710

Müller TM, Böttcher C, Morbitzer R, Götz CC, Lehmann J, Lahaye T, Glawischnig E (2015) TRANSCRIPTION ACTIVATOR-LIKE EFFECTOR NUCLEASE-Mediated Generation and Metabolic Analysis of Camalexin-Deficient *cyp71a12 cyp71a13* Double Knockout Lines. Plant Physiology **168:** 849-858

Munzert KS, Engelsdorf T (2025) Plant cell wall structure and dynamics in plant–pathogen interactions and pathogen defence. Journal of Experimental Botany **76:** 228-242

Nakagawa Y, Katagiri T, Shinozaki K, Qi Z, Tatsumi H, Furuichi T, Kishigami A, Sokabe M, Kojima I, Sato S, Kato T, Tabata S, Iida K, Terashima A, Nakano M, Ikeda M, Yamanaka T, Iida H (2007) Arabidopsis plasma membrane protein crucial for Ca2+ influx and touch sensing in roots. Proceedings of the National Academy of Sciences **104:** 3639-3644

Nakaminami K, Okamoto M, Higuchi-Takeuchi M, Yoshizumi T, Yamaguchi Y, Fukao Y, Shimizu M, Ohashi C, Tanaka M, Matsui M, Shinozaki K, Seki M, Hanada K (2018) AtPep3 is a hormone-like peptide that plays a role in the salinity stress tolerance of plants. Proceedings of the National Academy of Sciences **115:** 5810-5815

Narusaka Y, Narusaka M, Park P, Kubo Y, Hirayama T, Seki M, Shiraishi T, Ishida J, Nakashima M, Enju A, Sakurai T, Satou M, Kobayashi M, Shinozaki K (2004) RCH1, a locus in Arabidopsis that confers resistance to the hemibiotrophic fungal pathogen *Colletotrichum higginsianum*. Molecular Plant-Microbe Interactions **17:** 749-762

Nawrath C, Métraux J-P (1999) Salicylic Acid Induction–Deficient Mutants of Arabidopsis Express PR-2 and PR-5 and Accumulate High Levels of Camalexin after Pathogen Inoculation. The Plant Cell **11:** 1393-1404

Nomura H, Komori T, Kobori M, Nakahira Y, Shiina T (2008) Evidence for chloroplast control of external Ca2+-induced cytosolic Ca2+ transients and stomatal closure. The Plant Journal **53:** 988-998

Nomura H, Komori T, Uemura S, Kanda Y, Shimotani K, Nakai K, Furuichi T, Takebayashi K, Sugimoto T, Sano S, Suwastika IN, Fukusaki E, Yoshioka H, Nakahira Y, Shiina T (2012)

Chloroplast-mediated activation of plant immune signalling in Arabidopsis. Nature Communications **3:** 926

Novaković L, Guo T, Bacic A, Sampathkumar A, Johnson KL (2018) Hitting the Wall—Sensing and Signaling Pathways Involved in Plant Cell Wall Remodeling in Response to Abiotic Stress. Plants **7:** 89

O'Connell R, Herbert C, Sreenivasaprasad S, Khatib M, Esquerré-Tugayé M-T, Dumas B (2004) A novel Arabidopsis-*Colletotrichum* pathosystem for the molecular dissection of plant-fungal interactions. Molecular Plant-Microbe Interactions **17:** 272-282

Ortiz-Morea FA, Liu J, Shan L, He P (2022) Malectin-like receptor kinases as protector deities in plant immunity. Nature Plants **8:** 27-37

Paredez AR, Somerville CR, Ehrhardt DW (2006) Visualization of cellulose synthase demonstrates functional association with microtubules. Science **312:** 1491-1495

Pastorczyk M, Kosaka A, Piślewska-Bednarek M, López G, Frerigmann H, Kułak K, Glawischnig E, Molina A, Takano Y, Bednarek P (2020) The role of CYP71A12 monooxygenase in pathogen-triggered tryptophan metabolism and Arabidopsis immunity. New Phytologist **225:** 400-412

Perraki A, Gronnier J, Gouguet P, Boudsocq M, Deroubaix A-F, Simon V, German-Retana S, Legrand A, Habenstein B, Zipfel C, Bayer E, Mongrand S, Germain V (2018) REM1.3's phospho-status defines its plasma membrane nanodomain organization and activity in restricting PVX cell-to-cell movement. PLOS Pathogens **14:** e1007378

Reckleben L, Morton RN, Munzert-Eberlein KS, Thiel S, Rautengarten C, Tan V, Harres KL, Zanoni L, Ebert B, Engelsdorf T (2025) Galactan mobilization during carbon starvation compromises plant cell wall-mediated resistance to fungal infection. The Plant Journal **123:** e70438

Rhodes J, Yang H, Moussu S, Boutrot F, Santiago J, Zipfel C (2021) Perception of a divergent family of phytocytokines by the Arabidopsis receptor kinase MIK2. Nature Communications **12:** 705

Rohr L, Ehinger A, Rausch L, Glöckner Burmeister N, Meixner AJ, Gronnier J, Harter K, Kemmerling B, zur Oven-Krockhaus S (2024) OneFlowTraX: a user-friendly software for super-resolution analysis of single-molecule dynamics and nanoscale organization. Frontiers in Plant Science **15:** 1358935

Saga H, Ogawa T, Kai K, Suzuki H, Ogata Y, Sakurai N, Shibata D, Ohta D (2012) Identification and characterization of ANAC042, a transcription factor family gene involved in the regulation of camalexin biosynthesis in Arabidopsis. Molecular Plant-Microbe Interactions **25:** 684-696

Schindelin J, Arganda-Carreras I, Frise E, Kaynig V, Longair M, Pietzsch T, Preibisch S, Rueden C, Saalfeld S, Schmid B, Tinevez J-Y, White DJ, Hartenstein V, Eliceiri K, Tomancak P, Cardona A (2012) Fiji: an open-source platform for biological-image analysis. Nature Methods **9:** 676-682

Schmidt A, Mächtel R, Ammon A, Engelsdorf T, Schmitz J, Maurino VG, Voll LM (2020) Reactive oxygen species dosage in Arabidopsis chloroplasts can improve resistance towards Colletotrichum higginsianum by the induction of WRKY33. New Phytologist **226:** 189-204

Schoenaers S, Vissenberg K (2025) Overlooked aspects of CrRLK1L–RALF signaling. New Phytologist

Shen W, Liu J, Li J-F (2019) Type-II metacaspases mediate the processing of plant elicitor peptides in Arabidopsis. Molecular Plant **12:** 1524-1533

Tanaka K, Choi J, Stacey G (2013) Aequorin Luminescence-Based Functional Calcium Assay for Heterotrimeric G-Proteins in Arabidopsis. *In* MP Running, ed, G Protein-Coupled Receptor Signaling in Plants: Methods and Protocols. Humana Press, Totowa, NJ, pp 45-54

Tang J, Han Z, Sun Y, Zhang H, Gong X, Chai J (2015) Structural basis for recognition of an endogenous peptide by the plant receptor kinase PEPR1. Cell Research **25:** 110-120

Vaahtera L, Schulz J, Hamann T (2019) Cell wall integrity maintenance during plant development and interaction with the environment. Nature Plants **5:** 924-932

Van der Does D, Boutrot F, Engelsdorf T, Rhodes J, McKenna JF, Vernhettes S, Koevoets I, Tintor N, Veerabagu M, Miedes E, Segonzac C, Roux M, Breda AS, Hardtke CS, Molina A, Rep M, Testerink C, Mouille G, Höfte H, Hamann T, Zipfel C (2017) The Arabidopsis leucine-rich repeat receptor kinase MIK2/LRR-KISS connects cell wall integrity sensing, root growth and response to abiotic and biotic stresses. PLOS Genetics **13:** e1006832

Völkner C, Holzner LJ, Day PM, Ashok AD, Vries Jd, Bölter B, Kunz H-H (2021) Two plastid POLLUX ion channel-like proteins are required for stress-triggered stromal Ca2+release. Plant Physiology **187:** 2110-2125

Voll LM, Zell MB, Engelsdorf T, Saur A, Wheeler MG, Drincovich MF, Weber APM, Maurino VG (2012) Loss of cytosolic NADP-malic enzyme 2 in Arabidopsis thaliana is associated with enhanced susceptibility to *Colletotrichum higginsianum*. New Phytologist **195:** 189-202

von Arx M, Xhelilaj K, Schulz P, zur Oven-Krockhaus S, Gronnier J (2024) Photochromic reversion enables long-term tracking of single molecules in living plants. bioRxiv**:** 2024.2004.2010.585335

Weinl S, Held K, Schlücking K, Steinhorst L, Kuhlgert S, Hippler M, Kudla J (2008) A plastid protein crucial for Ca2+-regulated stomatal responses. New Phytologist **179:** 675-686

Wolf S (2022) Cell Wall Signaling in Plant Development and Defense. Annual Review of Plant Biology **73:** 323-353

Yamaguchi Y, Huffaker A, Bryan AC, Tax FE, Ryan CA (2010) PEPR2 Is a Second Receptor for the Pep1 and Pep2 Peptides and Contributes to Defense Responses in Arabidopsis The Plant Cell **22:** 508-522

Yamaguchi Y, Pearce G, Ryan CA (2006) The cell surface leucine-rich repeat receptor for *At*Pep1, an endogenous peptide elicitor in Arabidopsis, is functional in transgenic tobacco cells. Proceedings of the National Academy of Sciences **103:** 10104-10109

Zhai K, Rhodes J, Zipfel C (2024) A peptide-receptor module links cell wall integrity sensing to pattern-triggered immunity. Nature Plants **10:** 2027-2037

Zhang C, Wu Y, Liu J, Song B, Yu Z, Li J-F, Yang C, Lai J (2025) SUMOylation controls peptide processing to generate damage-associated molecular patterns in Arabidopsis. Developmental Cell **60:** 696-705.e694

Zhang Z, Gigli-Bisceglia N, Li W, Li S, Wang J, Liu J, Testerink C, Guo Y (2024) SCOOP10 and SCOOP12 peptides act through MIK2 receptor-like kinase to antagonistically regulate Arabidopsis leaf senescence. Molecular Plant **17:** 1805-1819

Zhou J, Mu Q, Wang X, Zhang J, Yu H, Huang T, He Y, Dai S, Meng X (2022) Multilayered synergistic regulation of phytoalexin biosynthesis by ethylene, jasmonate, and MAPK signaling pathways in Arabidopsis. The Plant Cell **34:** 3066-3087

Zhou J, Wang X, He Y, Sang T, Wang P, Dai S, Zhang S, Meng X (2020) Differential phosphorylation of the transcription factor WRKY33 by the protein kinases CPK5/CPK6 and MPK3/MPK6 cooperatively regulates camalexin biosynthesis in Arabidopsis. The Plant Cell **32:** 2621-2638

Figures

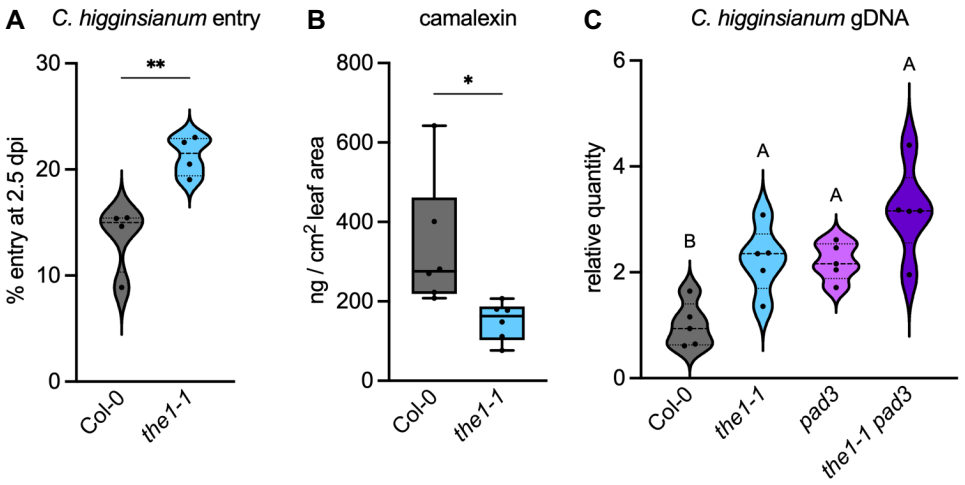

Figure 1: THE1 and camalexin biosynthesis have overlapping roles in resistance to *Colletotrichum higginsianum* infection.
(A) Entry rate of *C. higginsianum* on Col-0 and *the1-1* leaves at 2.5 days post infection (dpi) (n=4). (B) Camalexin amount in infected Col-0 and *the1-1* leaves at 2.5 dpi (n=6). Asterisks in (A,B) indicate statistically significant differences to Col-0 according to a Student's t-test (*$p < 0.05$, **$p < 0.01$). (C) The relative quantity of *C. higginsianum* DNA was determined at 4 dpi in Col-0, *the1-1*, *pad3* and *the1-1 pad3* (n=5). Different letters indicate statistically significant differences according to one-way ANOVA and Holm-Sidak's multiple comparisons test ($\alpha = 0.05$).

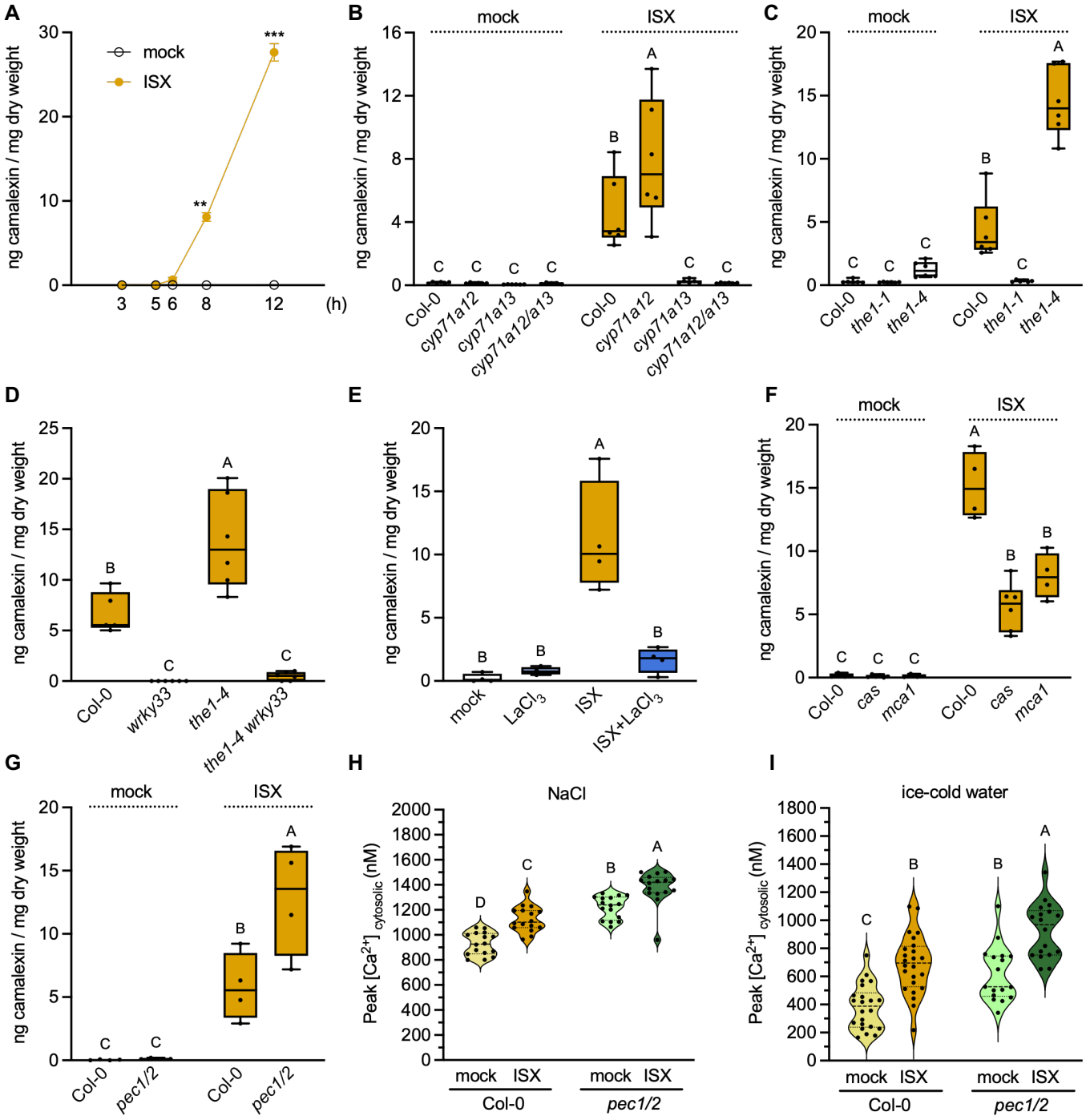

Figure 2: Isoxaben induces camalexin accumulation via THESEUS1, WRKY33 and calcium signaling. (A) Camalexin amount in Col-0 seedlings was determined at 3, 5, 6, 8 and 12 h after mock and isoxaben (ISX) treatment (n=3). Error bars indicate the SEM. Asterisks indicate statistically significant differences between ISX and mock according to a Student's t-test (*p < 0.05, **p < 0.01, ***p < 0.001). (B-G) Camalexin amount in (B) Col-0, *cyp71a12*, *cyp71a13* and *cyp71a12/a13* at 8 h after mock and ISX (n=5-6); (C) Col-0, *the1-1* and *the1-4* at 8 h after mock and ISX (n=6); (D) Col-0, *wrky33*, *the1-4* and *the1-4 wrky33* at 8 h after ISX (n=5-6); (E) Col-0 at 8 h after mock, $LaCl_3$, ISX and ISX+$LaCl_3$ (n=4); (F) Col-0, *cas* and *mca1* at 8 h after mock and ISX (n=4-6) and (G) Col-0 and *pec1/2* at 8 h after mock and ISX treatment (n=4). (H,I) Peak cytosolic Ca^{2+} values of transients in Col-0 and *pec1/2* seedlings after elicitation with (H) 200 mM NaCl (n=16) and (I) ice-cold water (n=17-24). Prior to elicitation, seedlings were treated for 4.5 h with mock or ISX. Different letters indicate statistically significant differences according to (D,E) one-way ANOVA or (B,C,F,G,H,I) two-way ANOVA and Holm-Sidak's multiple comparisons test (α = 0.05).

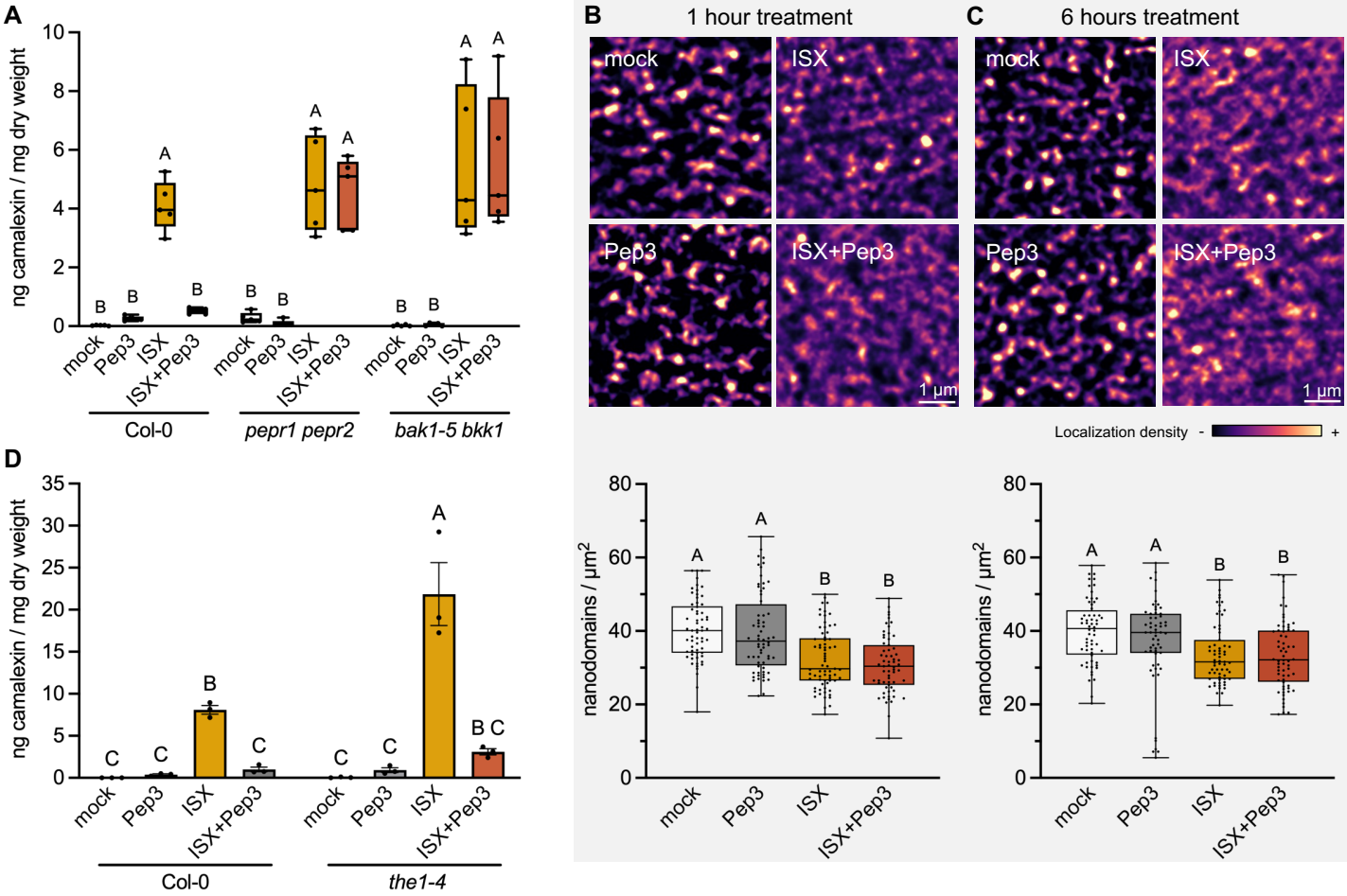

Figure 3: Pep3-PEPR signaling impairs induction of camalexin synthesis downstream of THE1. (A) Camalexin amount in Col-0, *pepr1 pepr2* and *bak1-5 bkk1* seedlings at 8 h after mock, Pep3, isoxaben (ISX) and ISX+Pep3 treatment (n=5). Different letters indicate statistically significant differences according to two-way ANOVA and Holm-Sidak's multiple comparisons test (α = 0.05). (B,C) THE1-GFP nanodomain density was determined in seedling hypocotyls at (B) 1 h and (C) 6 h after treatment with mock, Pep3, ISX and ISX+Pep3. Representative images of enhanced super-resolution radial fluctuation (eSRRF) analysis are shown alongside the quantification of nanodomain density in 3 pooled experiments with 4-8 cells from 3 seedlings per experiment (n=58-69). Different letters indicate statistically significant differences according to Kruskal-Wallis and Dunn's test (α = 0.05). (D) Camalexin amount in Col-0 and *the1-4* seedlings at 8 h after mock, Pep3, ISX and ISX+Pep3 treatment (n=3). Error bars indicate the SEM. Different letters indicate statistically significant differences according to two-way ANOVA and Holm-Sidak's multiple comparisons test (α = 0.05).

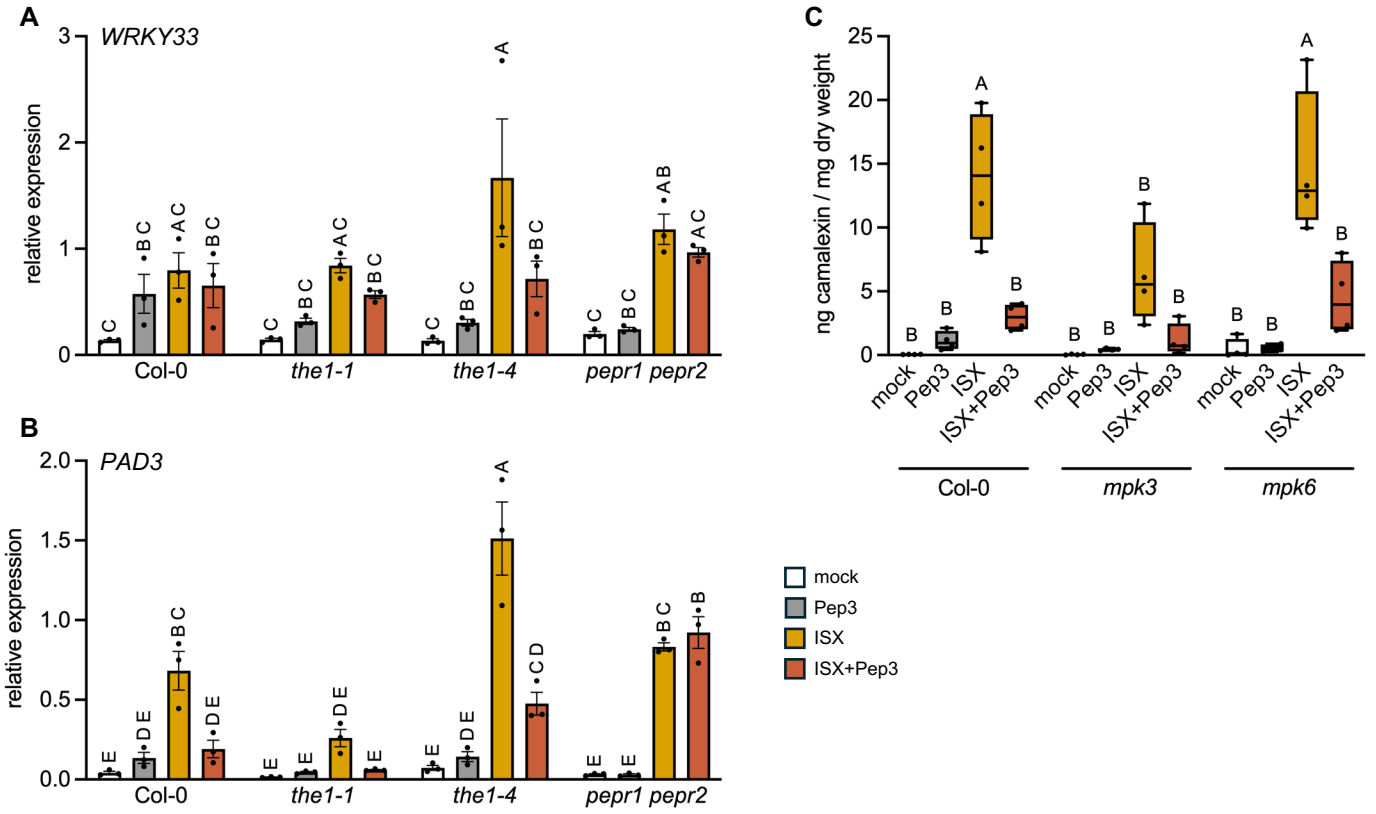

Figure 4: Pep3-dependent inhibition of CWI signaling does not involve WRKY33 and MPK3/6. Relative expression of (A) *WRKY33* and (B) *PAD3* was determined in Col-0, *the1-1*, *the1-4* and *pepr1 pepr2* at 6 h after treatment with mock, Pep3, isoxaben (ISX) and ISX+Pep3 via quantitative RT-PCR. Values are relative to *ACT2* expression and error bars represent the SEM (n=3). (C) Camalexin amount in Col-0, *mpk3* and *mpk6* seedlings at 8 h after mock, Pep3, ISX and ISX+Pep3 treatment (n=4). Different letters indicate statistically significant differences according to two-way ANOVA and Holm-Sidak's multiple comparisons test (α = 0.05).

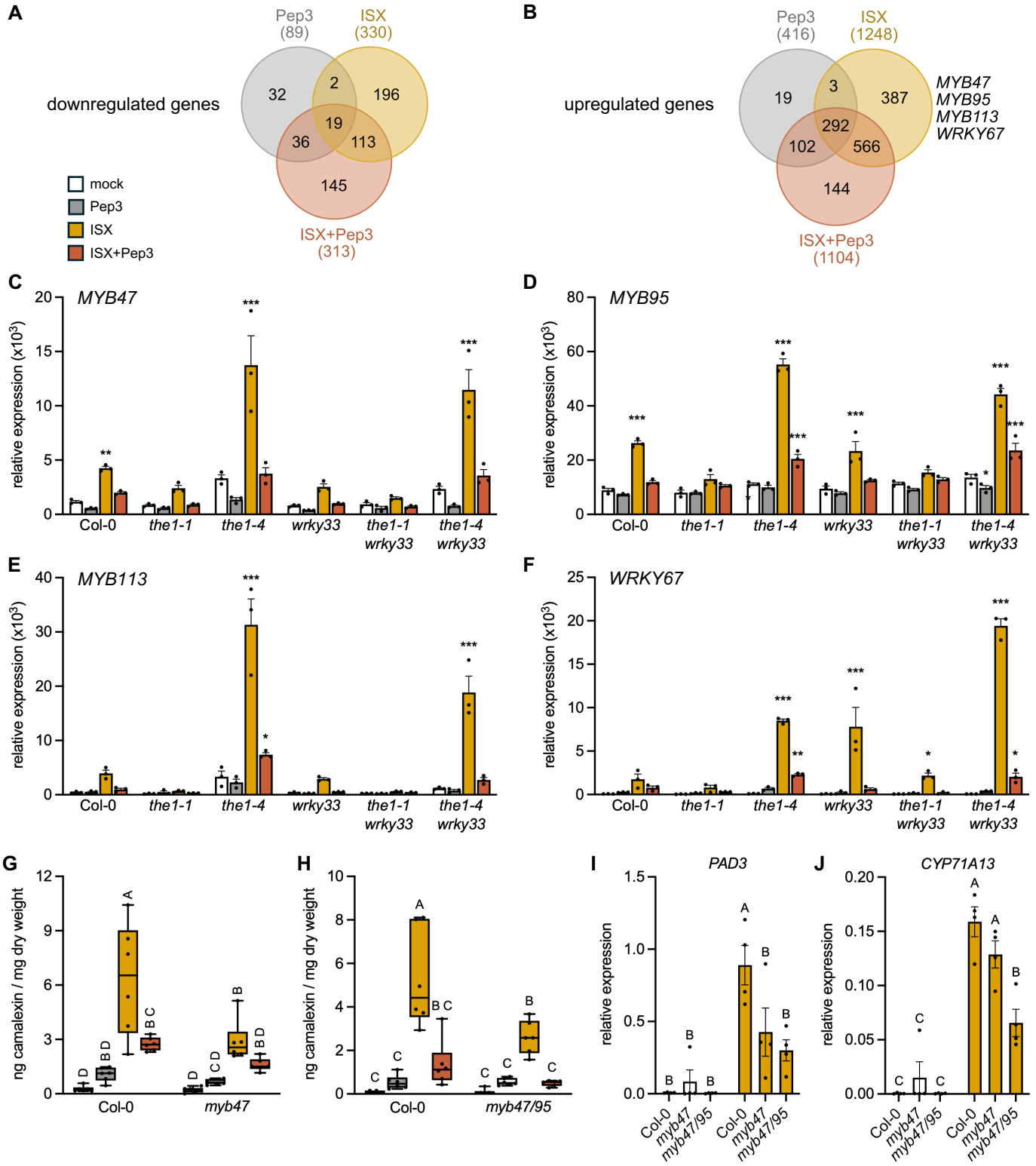

Figure 5: Identification of Pep3-regulated transcription factors involved in ISX-induced camalexin accumulation.

(A, B) RNA-Sequencing of Col-0 seedlings identifies genes (A) upregulated and (B) downregulated at 6 h after treatment with mock, Pep3, isoxaben (ISX) and ISX+Pep3 (α = 0.05, fold change >2). (C-F) Relative expression of (B) *MYB47*, (C) *MYB95,* (D) *MYB113* and (E) *WRKY67* was determined in Col-0, *the1-1*, *the1-4, wrky33, the1-1 wrky33* and *the1-4 wrky33* at 6 h after treatment with mock, Pep3, ISX and ISX+Pep3 via quantitative RT-PCR. Values are relative to *ACT2* expression and error bars represent the SEM (n=3). Asterisks indicate statistically significant differences to the respective mock treatments according to two-way ANOVA and Holm-Sidak's multiple comparisons test (*p < 0.05, **p < 0.01, ***p < 0.001). (G,H) Camalexin amount in (G) Col-0 and *myb47,* and in (H) Col-0 and *myb47/95* seedlings at 8 h after mock, Pep3, ISX and ISX+Pep3 treatment (n=6). (I,J) Relative expression of (I) *PAD3* and (J) *CYP71A13* was determined in Col-0, *myb47* and *myb47/95* seedlings at 8 h after treatment with mock and ISX via quantitative RT-PCR. Values in are relative to *ACT2* expression and error bars represent the SEM (n=4). Different letters in (G-J) indicate statistically significant differences according to two-way ANOVA and Holm-Sidak's multiple comparisons test (α = 0.05).

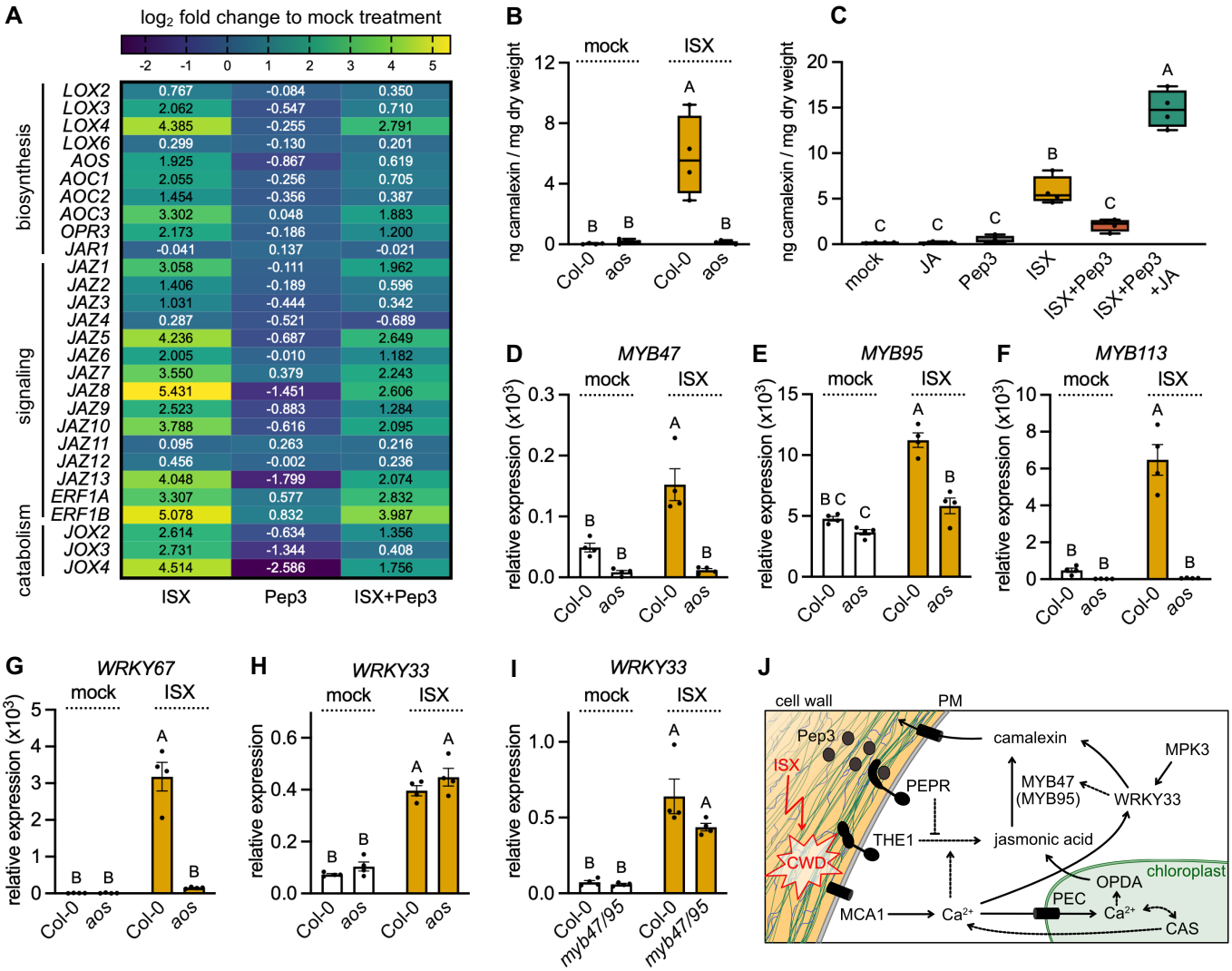

Figure 6: ISX-induced and Pep3-sensitive camalexin accumulation depends on jasmonic acid. (A) Transcripts involved in jasmonic acid (JA) biosynthesis, signaling and catabolism were analyzed via RNA-Sequencing in Col-0 seedlings treated with mock, Pep3, isoxaben (ISX) and ISX+Pep3 for 6 h. Relative expression after ISX, Pep3 and ISX+Pep3 compared to mock treatment is listed as $\log_2$ fold change and visualized as heat map indicating downregulation (dark blue) and upregulation (yellow) of transcripts. (B, C) Camalexin amount in (B) Col-0 and *aos* seedlings at 8 h after mock and ISX treatment (n=4-5) and (C) Col-0 seedlings at 8 h after mock, JA, Pep3, ISX, ISX+Pep3 and ISX+Pep3+JA treatment (n=4). (D-G) Relative expression of (D) *MYB47*, (E) *MYB95,* (F) *MYB113* and (G) *WRKY67* was determined in Col-0 and *aos* seedlings at 6 h after treatment with mock and ISX via quantitative RT-PCR. (H,I) Relative expression of *WRKY33* was determined in (H) Col-0 and *aos* and (I) Col-0 and *myb47/95* seedlings at 6 h after treatment with mock and ISX via quantitative RT-PCR. Values in (D-I) are relative to *ACT2* expression and error bars represent the SEM (n=4). Different letters indicate statistically significant differences according to (C) one-way ANOVA or (B,D-I) two-way ANOVA and Holm-Sidak's multiple comparisons test (α = 0.05). (J) Model depicting the induction of camalexin synthesis after perception of cell wall damage (CWD) via THE1, JA and MYB47/95. Interactions with Pep3/PEPR-, WRKY33-, and Ca^{2+} signaling are proposed based on data presented in this manuscript and references discussed in the main text.